Comments

We thank the reviewers and the co-editor for their valuable comments. The replies are in blue.

General comment:

R1. Many figures show yields vs SOA mass loading. I assume that the SOA mass loading corresponds to the resulting SOA using different concentrations of precursors (alpha-pinene etc), and not to seed aerosol loading. – Is this correct?

Reply. Yes. The SOA mass loading corresponds to the SOA mass formed when the different concentrations of precursor gas is oxidized and not the seed aerosol loadings.

R2. Could you add to the figures the information what precursor concentrations have been used to obtain the SOA mass yields? For example, I assume that the different 'branches' in Figure 6 correspond to different initial alpha-pinene concentrations (0.5 – 200 ppb)? Would the figure look the same if you plotted yield vs initial precursor concentration? – I'm not suggesting presenting all figures like this, but I'm just trying to understand it.

Reply. The information of initial concentrations of precursor gas has been added to the figure 6 caption. The different branches in Figure 6 correspond to different NO concentrations which is varied between 0-5 ppb. So each branch represents mass loadings for varying α-pinene and O_3 concentrations but constant NO concentrations. For example, the black diamonds correspond to mass yields from ozonolysis of different concentrations of α-pinene (0.5-200ppb) and constant NO concentration of 0.5ppb. If the figure is plotted with initial precursor concentration on the x-axes we get the following plot. For each concentration of α-pinene (eg 5ppb) we have 5 yield points corresponding to 5 values of O_3 concentrations (1.0, 5.0,10.0, 50.0,100.0 in the unit of 10^{11} #cm^{-3}).

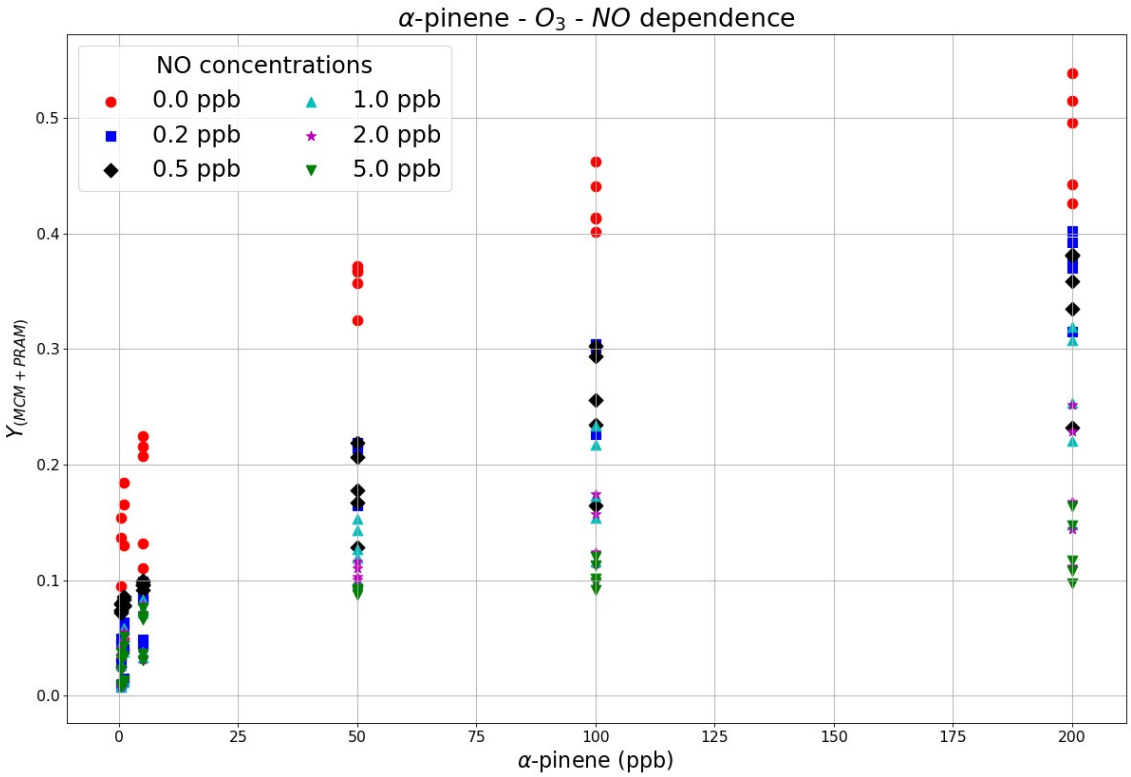

Figure C1. Concentration vs Mass yields

R3. Please use consistent descriptions on the y-axes (either Y or 'mass yields')

Reply. Done. The figures descriptions on the y axes are now consistent (Figure 6 and 8).

l. 65: Define MW

Reply. Done.

l. 113: Why is Table 1c cited before the other Table parts? – I think it is rather unusual anyway to have multiple Table parts (a, b, c), but I leave it up to you to or to the copy editing service to change it or not.

Reply. Changed. The Table 1c is now cited later in a more appropriate context in the text. We follows the citing sequence of Table 1a,b and c.

l. 209: The x-axis of the figure seems to only show a range of < 100 (~800?).

Reply. Yes, That was a typo in the text.

l. 232: replace 'value' by 'yield'

Reply. Done.

l. 252: ‘ozonolysis’ misspelled

Reply. Corrected

l. 268: Add the value measured by Lee et al (0.58?)

Reply. Done.

l. 281: Do you mean ‘Figure 3’? (Fig. 2 shows ozone oxidation.)

Reply. Yes. Corrected.

l. 313: Shouldn’t it just read ‘... from application of MCM’ as PRAM is not available for NO_3 reactions? – If so, please also change the header of the figure.

Reply. Done.

l. 400: Shouldn’t that be 99% (as in the SI, you list 98.59%)?

Reply. Yes. Changed.

l. 567: Please replace by citation of ACP (not ACPD) paper.

Reply. Done.

l. 622: Reference is incomplete

Reply. Changed.

l. 644: Update reference.

Reply. Done.

l. 685: Incomplete.

Reply. Changed.

Supplement material

Table 1s a- c: Add to the table captions that it is for the oxidation of alpha-pinene by ozone

Reply. Done.

l. 28, 34 and 41: Should be called ‘Figure 4s’

Reply. Yes. Changed.

l. 36: The reference to Figure 9 seems wrong here. Do you mean Figure 4s?

Reply. Yes. Changed.

Aerosol Mass yields of selected Biogenic Volatile Organic Compounds – a theoretical study with near explicit gas-phase chemistry

Carlton Xavier[1], Anton Rusanen[1], Putian Zhou[1], Chen Dean[1], Lukas Pichelstofer[1], Pontus Roldin[2], Michael Boy[1]

[1]Institute for Atmospheric and Earth Systems Research (INAR), Physics, University of Helsinki

[2]Division of Nuclear Physics, Lund University, Box 118, SE-22100, Lund, Sweden

Correspondence : Carlton Xavier (carlton.xavier@helsinki.fi), Michael Boy (michael.boy@helsinki.fi)

Abstract

In this study we modeled secondary organic aerosols (SOA) mass loadings from the oxidation (by O_3, OH and NO_3) of five representative Biogenic Volatile Organic compounds (BVOCs): isoprene, endocyclic bond containing monoterpenes (α-pinene and limonene), exocyclic double bond compound (β-pinene) and a sesquiterpene (β-caryophyllene). The simulations were designed to replicate idealized smog chamber and oxidative flow reactors (OFR). The master chemical mechanism (MCM) together with the peroxy radical autoxidation mechanism (PRAM), were used to simulate the gas-phase chemistry. The aim of this study was to compare the potency of MCM and MCM+PRAM in predicting SOA formation. SOA yields were in good agreement with experimental values for chamber simulations when MCM+PRAM was applied, while a standalone MCM under-predicted the SOA yields. Compared to experimental yields, the OFR simulations using MCM+PRAM yields were in good agreement for BVOCs oxidized by both O_3 and OH. On the other hand, a standalone MCM under-predicted the SOA mass yields. SOA yields increased with decreasing temperatures and NO concentrations and vice-versa. This highlights the limitations posed when using fixed SOA yields in a majority of global and regional models. Few compounds that play a crucial role (>95% of mass load) in contributing to SOA mass increase (using MCM+PRAM) are identified. The results further emphasized that incorporating PRAM in conjunction with MCM does improve SOA mass yields estimation.

1. Introduction

Atmospheric secondary organic aerosols, formed from gas to particle phase conversion of the oxidation products of volatile organic compounds (VOC) significantly impact the organic aerosol mass loadings (Griffin, 1999; Kanakidou et al., 2005). However, the scale of SOA contribution to the aerosol particle mass is still subject to high uncertainties (Hao et al., 2011,Glasius and Goldstein, 2016). The elevated aerosol particle concentrations are shown to have inimical effects on health (Miller et al., 2007), and a varying degree of influence on the climate by forming cloud condensation nuclei (CCN), altering the cloud properties

and radiative balance (Rosenfeld et al., 2014; Schmale et al., 2018). Therefore, it is acutely necessary to understand the role and contributions of SOA to the particle loading in the atmosphere. Biogenic VOCs from forest are estimated to contribute to about 90% of VOCs emissions globally (Guenther et al., 1995, 1999 and 2000). The most important BVOCs for SOA formation are isoprene (C_5H_8), monoterpenes ($C_{10}H_{16}$) and sesquiterpenes ($C_{15}H_{24}$). These compounds are all alkenes containing at least one carbon-carbon double bond, enabling them to undergo oxidation by the dominant atmospheric oxidants: the hydroxyl radical (OH), ozone (O_3) and the nitrate radical (NO_3). For some of the terpenes, initial oxidation steps can lead to formation of highly oxygenated organic molecules (HOM). These HOMs generally have low volatilities and can condense nearly irreversibly, thereby producing SOA (Ehn et al., 2014). HOMs, detected in both the ambient atmosphere and chamber experiments (Ehn et al., 2012) are formed by autoxidation (Berndt et al., 2016; Crounse and Nielsen, 2013) wherein peroxy radicals (RO_2) undergo subsequent intramolecular H-shifts accompanied by rapid reactions with O_2. Autoxidation hence results in compounds containing multiple functional groups such as hydroxyls, peroxides and carbonyls (Bianchi et al., 2017,Bianchi et al., 2019).

A majority of chamber and flow-tube experiments have focused on HOM formation from the oxidation of various VOCs and their contribution to SOA mass loadings (Ehn et al., 2014; Kristensen et al., 2017). Oxidation of isoprene (Liu et al., 2016), endocyclic monoterpenes containing reactive double bonds such as α-pinene and limonene (Zhao et al., 2015) , or exocyclic double bond containing compounds such as β-pinene (Jokinen et al., 2015) and sesquiterpenes such as β-caryophyllene (Chen et al., 2012) have been investigated. The SOA forming potential of various BVOCs depends on the isomeric structures (Friedman and Farmer, 2018; Keywood et al., 2004). Ozonolysis of compounds containing reactive endocyclic bonds such as α-pinene produce higher SOA mass yields of 41% in comparison to those with exocyclic bonds (β-pinene), which produce mass yields of 17 % (Lee et al., 2006a). One explanation for this dependence on the isomeric structure is attributed to the formation of HOMs (Ehn et al., 2014). Another important factor influencing HOM formation is the initial oxidant, as pointed out by Zhao and co-workers (2015). They showed that the SOA formation by OH oxidation of α-pinene and limonene were lower when compared to their SOA formed by ozonolysis. Further they measured lower H/C ratio for SOA produced by monoterpene ozonolysis (experiments were carried out in dark with CO as OH scavenger), in comparison to OH oxidation of α-pinene and limonene, while O/C ratio were similar for both oxidation cases. This was attributed to the formation of RO_2 radicals (monoterpenes $+O_3$) which undergo internal hydrogen shifts and subsequently react with another RO_2 radical, to form compounds containing carbonyl groups while losing hydrogen atoms in the process. A similar analysis was conducted by Draper et al. (2015), who showed that an increase in NO_2 concentration reduced α-pinene ozonolysis SOA mass yields, while no appreciable reduction in mass yields

153 are reported for β-pinene and Δ^3- carene ozonolysis. On the other hand, the mass yields from limonene
154 ozonolysis increased with increasing NO_2 concentrations (Draper et al., 2015). This disparity in mass yields
155 for different BVOCs in the presence of NO_2 is possibly caused by the formation of high molecular weight
156 oligomers (or lack of in case of α-pinene) through oxidation with NO_3 that contribute to SOA mass loadings
157 (Draper et al., 2015).

158 Due to computational limitations, many regional and canopy scale atmospheric chemistry models
159 generally use isoprene and/or a representative monoterpene (generally α-pinene), to model SOA yields
160 (Friedman and Farmer, 2018). The SOA yields of different monoterpenes vary with structure, NO_x and
161 temperature (Friedman and Farmer, 2018; Kristensen et al., 2017; Presto et al., 2005). This poses a limitation
162 on using representative monoterpene fixed SOA yields in many of the global models and increases
163 uncertainties in predicting cloud condensation nuclei concentrations, cloud droplet number concentrations and
164 radiative balance due to aerosol loadings.

165 This work aims to investigate the SOA mass loading from the oxidation products of BVOCs with the
166 atmospheric oxidants OH, O_3 and NO_3 with a specific focus on the BVOCs isoprene, α-pinene, β-pinene,
167 limonene and β-caryophyllene. Further we study the effect of varying temperature (258.15 K – 313.15 K) and
168 NO concentrations (0 - 5 ppb) on α-pinene oxidation mass yields. We use the master chemical mechanism
169 (MCMv3.3.1) (Jenkin et al., 1997, 2012 and 2015; Saunders et al., 2003), a near explicit gas-phase chemical
170 mechanism together with peroxy radical autoxidation mechanism (PRAM, Roldin et al., 2019) (PRAM +
171 MCM). The aim is to understand the importance and contribution of peroxy radical autoxidation products to
172 the SOA mass yields from terpenes.

173

174 ## 2. **Model description**

175 ### 2.1 **Malte Box**

176 MALTE (Model to predict new Aerosol formation in Lower TropospherE) is a one-dimensional
177 model consisting of modules calculating boundary layer meteorology, emissions of BVOCs, gas-phase
178 chemistry and aerosol dynamics with the aim to simulate particle distribution and growth in the lower
179 troposphere (Boy et al., 2006). In this study, a zero-dimensional version, MALTE-Box is applied to simulate
180 an ideal chamber and flow-tube environment (i.e. no wall losses effects are considered in this study). For the
181 simulations performed in this study the emission module was switched off while only employing the gas-
182 phase chemistry and aerosol dynamics module.

Kinetic preprocessor (KPP) is used to generate a system of coupled differential equations to solve the gas-phase chemistry schemes (Damian et al., 2002). The peroxy radical autoxidation mechanism (PRAM), (Roldin et al., 2019, Qi et al., 2018, Öström et al., 2017), formulated based on the oxidation of monoterpenes as described by Ehn et al. (2014) was incorporated alongside MCMv3.3.1. PRAM explicitly describes the formation and evolution of peroxy radicals (RO_2) from the ozonolysis and OH oxidation of monoterpenes, driven by subsequent H-shifts and O_2 additions. The current version of PRAM based on experimental and theoretical studies, considers HOM autoxidation for a fraction of the peroxy radicals formed during the ozonolysis of α-pinene and limonene and OH oxidation of α-pinene, β-pinene and limonene. This is achieved by assigning species specific molar yields for the formation of first RO_2, which subsequently initiates the autoxidation chain (Roldin et al., 2019). Currently, in PRAM a maximum first generation RO_2 yield of 9% for α-pinene ozonolysis, 21.9 % for limonene ozonolysis, 2.5 % for α-pinene+OH, and 1% for both limonene+OH and β-pinene+OH first generation products are allowed to initiate autoxidation (Roldin et al., 2019). For β-pinene ozonolysis the molar yield of RO_2 is minor (<0.1 %) (Roldin et al., 2019, Ehn et al. 2014) and hence not considered in this work. The above mentioned RO_2 molar yields used in this work are close to the experimental values obtained in both smog chamber and flow tube experiments. Ehn et al. (2014) measured an RO_2 yield of ~7% for α-pinene ozonolysis and ~17% for limonene ozonolysis, whereas Jokinen et al. (2015) measured 0.58 % and 0.93 % for OH oxidation of β-pinene and limonene respectively. The autoxidation is terminated by bimolecular reactions, wherein the RO_2 formed reacts with NO, HO_2 or other peroxy radicals, thereby forming alkoxy radicals, closed shell monomers or dimers (Roldin et al., 2019). The PRAM considers temperature dependent autoxidation reaction rates, which is important when investigating the SOA mass yields at varying temperatures ~~(Table 1c)~~. The temperature dependence in PRAM is based on quantum chemical calculations wherein the autoxidation rates correspond to an activation energy of 24 kcal/mol. The activation energies vary for autoxidation of different RO_2 from α-pinene ozonolysis between 22 and 29 kcal/mol (Rissanen et al., 2015), leading to varying autoxidation rates at different temperatures (Roldin et al., 2019). It should be noted that the temperature dependence in PRAM is a first of its kind but needs further evaluation using recent measurements of HOM formation at different temperatures (e.g. Quéléver et al., 2019).

The aerosol dynamics are simulated using the University of Helsinki Multicomponent Aerosol model (UHMA) originally from Korhonen et al. (2004). The model has undergone significant development since then to allow simulation with all the compounds from MCM. It now supports an unlimited number of condensing vapors and solves condensation using the analytical predictor of condensation method from Jacobson (1997). The condensation algorithm considers both, the Kelvin effect and Raoult's law. The

processes included in the model are nucleation, condensation, evaporation, coagulation and deposition. The discretization of the size distribution and the time evolution is modeled with the moving section approach, with optional redistribution to a fixed grid. In this work, the redistribution is active to make the coagulation more accurate, since it requires that grid points are available near the size of the coagulated particles. In this study nucleation and deposition are not active, and hence are not considered. A total of 100 size bins ranging from 1nm to 20 µm with the fixed grid was applied for this study.

A group contribution method based on Nannoolal et al. (2008) using the UManSysProp online system (Topping et al., 2016) was used to estimate the pure liquid saturation vapor pressures (p_0) of the organic compounds in MCMv3.3.1. For the PRAM species, p_0 were estimated using the functional group method SIMPOL (Pankow and Asher, 2008; see Roldin et al., 2019 for details). Temperature was used as an input to estimate p_0 for both the group contribution methods.

2.2 **Simulations**

The simulations performed in this study are aimed to closely resemble an idealized smog chamber (batch mode setup) and an Oxidative Flow Reactor (OFR) without interactions between the gas phase and the system walls. For the chamber runs, the VOC and oxidants were introduced at the beginning (time, t=0 sec), set to certain concentrations (Table 1a) and then allowed to react. Both chamber and OFR simulations are performed using ammonium sulfate seed particles which are introduced at time t=0. The condensation sink (CS) was inferred from the size distribution of seed particles used in the model. The CS for the chamber and OFR simulations was set to 0.00067 s^{-1} and 0.067 s^{-1} respectively. SOA mass yields obtained using an OFR are sensitive to short residence time used, hence the seed particle surface area should be chosen in order to overcome the mass yield underestimation (Ahlberg et al., 2019). CS sensitivity runs (Supplement Figure S1) were performed for α-pinene-O_3 to determine the CS for which there are no appreciable change in mass yields with increasing particle surface.

The simulation for the chamber setup is run for a maximum time of 24 hours and ends when either of the 2 criteria are satisfied: (1) the simulation time reaches the 24-hour mark or (2) 90 % of the initial precursor VOC has reacted away. In the latter case the simulation is continued for an additional 2 hours to ensure enough time for the vapors to condense onto the seed particles. By contrast, the OFR runs were simulated for a maximum residence time of 100 seconds, ensuring all initial precursor vapors were oxidized. Seed particles were also added in the OFR simulations. The oxidant concentrations used for the OFR simulations (Table 1b) are significantly higher in comparison to the simulated chamber runs (~2 orders of magnitude larger). The time step for the chamber and flow-tube simulations are set to t=10 s and t =0.1 s

respectively. The runs performed were oxidant specific (i.e. VOCs would be oxidized by only one specific oxidant at any given time). For the O_3 specific simulations no OH could form in both, OFR and chamber setups, thus enabling oxidation of O_3 to be the only pathway.

The simulations were performed at atmospheric relevant NO_x (NO_x = NO +NO_2) concentrations, corresponding to [NO]=0.5 ppb and [NO_2] = 2.0 ppb conditions with the relative humidity (RH) set to 60 % and temperature to 293.15 K. The RH value considered in this study is based on previous published experimental studies performed at ~60 % in both smog chamber (Bruns et al., 2015a; Ehn et al., 2014; Stirnweis et al., 2017) and OFR (Ahlberg et al. et al., 2018). α-pinene ozonolysis runs were performed at four different temperatures: 258.15 K, 278.15 K, 303.15K and 313.15 K, respectively (Table 1c) . SOA mass yields are expected to increase with decreasing temperature (Saathoff and Naumann, 2009). A similar temperature dependence was observed by Kristensen et al. (2017) who observed SOA mass yield from α-pinene ozonolysis at ~ 40 % and ~20 % at 258 K and 293 K respectively. Analogous to analyzing the effect of varying temperature on SOA yields, we study the variation in α-pinene ozonolysis SOA mass yields by varying the NO_x concentrations (Table 1c) . SOA yields for α-pinene ozonolysis at high NO_x conditions should be suppressed (Ng and Chhabra, 2007), which could be due to the production of relatively, volatile organic nitrates under high NO_x conditions as compared to less volatile products during low NO_x conditions (Presto et al., 2005).

Furthermore, two different chemistry schemes were applied for the simulations. One scheme consisted of only the MCM chemistry mechanism and the second included the MCM+PRAM chemistry mechanism. Table 1a shows the concentrations of different BVOCs and Table 1b shows the oxidants concentrations used for the simulations.

Table 1a. Concentrations of different BVOCs

α-pinene (ppb)	**β-pinene (ppb)**	**Isoprene (ppb)**	**Limonene (ppb)**	**B-caryophyllene (ppb)**
0.5, 1.0, 5.0, 50.0, 100.0, 200.0	0.5, 1.0, 5.0, 50.0, 100.0, 200.0	5.0, 50.0, 100.0, 200.0	1.0, 5.0, 50.0, 100.0, 200.0	0.5, 1.0, 2.0, 5.0, 10.0

Table 1b. Concentrations of different oxidants for chamber and flow-tube runs

OH (* 10^6 #/cm^3) - chamber	**O_3 (* 10^{11} #/cm^3) - chamber**	**NO_3 (* 10^7 #/cm^3) - chamber**
OH (* 10^8 #/cm^3) - OFR	**O_3 (* 10^{13} #/cm^3) - OFR**	**NO_3 (* 10^9 #/cm^3) - OFR**

2.0, 5.0 ,10.0, 50.0,100.0	1.0, 5.0 ,10.0, 50.0,100.0	1.0, 5.0 ,10.0, 50.0,100.0

Table 1c. NO concentrations and temperatures used for α-pinene ozonolysis

NO (ppb)	0.5 (default), 0, 0.2, 1, 2, 5
Temperature (K)	293.15 (default), 258.15, 278.15, 303.15, 313.15

2.3 Mass Yields

The SOA mass yields (Y) are determined by calculating the ratio of the amount of SOA or mass concentration of organic aerosol formed (C_{OA}) to the amount of VOC (ΔVOC) reacted:

$$Y = \frac{C_{OA}}{\Delta VOC} \quad (1)$$

A volatility basis set is fit to the data to obtain the volatility distribution. In this study equilibrium partitioning was only assumed for deriving the volatility distribution based on the model simulations. Following Donahue et al. (2006), the SOA is assumed to be in equilibrium with the gas-phase and using the effective saturation concentration C_i^* spaced logarithmically. The individual product partitioning to the particle phase can be estimated using

$$E_i = \left(1 + \frac{C_i^*}{C_{OA}}\right)^{-1} \quad (2)$$

Where E_i is the fraction of species in the condensed particle phase. The above equation determines the fraction of species in the particle phase as well as in the gas phase. For example, if we assume C_{OA} =10 μg m^{-3} a species with C^* = 10 μg m^{-3} will partition 50 % to condensed phase and the rest 50% will reside in the gas phase. The fidelity of this equilibrium partitioning enables the parameterization of product vapors in volatility C^* bins that are near the C_{OA} concentrations (Henry et al., 2012).

3. Results and Discussion

SOA mass yields were simulated for the oxidation of various biogenic volatile organic compounds (isoprene, α-pinene, limonene and β-caryophyllene, β-pinene) by dominant atmospheric oxidants OH, O_3 and NO_3. The following section examines the comparison between the yields derived using MCM+PRAM and a standalone MCM for chamber and flow-tube experiments.

3.1 BVOCs – O_3 chamber and flow-tube simulations

In Fig. 1 panel A indicates the SOA mass yields derived on applying a coupled MCM+PRAM mechanism to ozonolysis of α-pinene and limonene (PRAM is only available for ozonolysis of α-pinene and limonene) and the lower panel B shows ratio of yields obtained by MCM and coupled MCM+PRAM.

The abscissa, depicted on a log scale, considers the entire range of SOA mass loadings from 1-~~1150~~ 800 μg m^{-3}. Each data point is representative of simulated SOA mass yields resulting from variable BVOC loading. The resulting mass yields for α-pinene in the range shown in Table 2a. are consistent with the yields found in various smog chamber experiments.The mass yields derived using MCM+PRAM for α-pinene ozonolysis are in good agreement with the experimental yields measured for similar mass loadings by Kristensen et al. (2017) and Pathak et al. (2007). The standalone MCM, on the other hand, severely under-predicts the mass yields for α-pinene ozonolysis. The MCM+PRAM also shows better agreement with experiments when estimating the lower range mass yields for SOA mass loadings of < 15 μg m^{-3}. This is supported by the values obtained by Shilling et al. (2008), where the authors measured a 0.09 yield from α-pinene ozonolysis for SOA mass loading of 10.6 μg m^{-3}. Limonene ozonolysis mass yields using MCM+PRAM in comparison to standalone MCM, are much closer to the values given by Waring (2016).

The formation of HOM from β-pinene ozonolysis is low (Ehn et al., 2014; Jokinen et al., 2015) and hence not considered in PRAM. The peroxy radical autoxidation mechanism for β-caryophyllene ozonolysis has not yet been developed and therefore, not considered in PRAM. When comparing the measured mass yield values for β-caryophyllene (Chen et al. 2012) and β-pinene ozonolysis (Griffin (1999) and Pathak et al. (2008)) to the modeled values using the MCM scheme, it is evident that the MCM scheme drastically under-predicts the SOA mass yields (Fig. 2).

Today oxidation flow reactor (OFR) experiments are complementing the traditional batch mode smog chamber experiments. The OFR generally exhibits lower mass yields compared to the smog chamber experiments at ranges of equivalent oxidant exposure (Lambe et al., 2015). We modeled flow-tube simulation after the potential aerosol mass (PAM) OFR, where the residence time is in the order of a few to several minutes (Lambe et al., 2011). The model simulations are performed with a maximum residence time of 100 seconds with O_3 exposures ranging from 1.0 x 10^{15} – 1.0 x 10^{17} molecules cm^{-3} s (residence time * [O_3]). Kang and Root (2007) measured a ~~value~~ yield of 0.2 for ozonolysis of α-pinene for an initial precursor VOC concentration of 100 ppbv, while we obtain ~0.25 (MCM+PRAM) for the similar initial precursor concentrations. The OFR yields for β-pinene (MCM-only) are significantly lower (0.02) than the values

measured by Kang and Root (2007) wherein they measured a yield of 0.49 for similar initial precursor concentrations. Addition of seed particles promotes condensation, leading to increased SOA yields (Lambe et al., 2015) which was confirmed by Ahlberg et al, (2019). Kang and Root (2007) found that using seed particles, the yield from α-pinene ozonolysis increased by a factor of ~1.4 which can explain our yields for α-pinene ozonolysis simulations. The mass spectra plot (Figure S2) shows that PRAM contributes the majority of dimers to the particle phase, while MCM dominate monomer contribution. Another interesting facet of Figure S2 are the different condensing compounds in both OFR and chamber simulations. The higher absolute RO_2 concentrations in the OFR simulations explain the lower concentration of HOM monomers and dimers relative to the chamber simulations, i.e. the high RO_2 concentrations in the OFR cause termination of the peroxy radical autoxidation chain before the RO_2 become highly oxygenated, thereby influencing SOA yields. Hence, this should be taken into account when using yields from OFR as inputs to regional and global models.

Table 2a. Mass yields for BVOCs ozonolysis at 293 K for different range of mass loadings using a chamber[†] setup. The values in parenthesis in the column 'Experimental yields' indicates the corresponding experimental mass loadings in unit of μg m^{-3}.

SOA mass loading (μg m^{-3})	**MCM + PRAM mass yields range**	**MCM mass yields range**	**BVOC**	**Experimental yields**	**References**
0– 15[†]	0.07– 0 .08	0.00 – 0.06	α-pinene	0.09 (10.6)	Shilling et al. (2008)
16 - 60[†]	0.12 – 0.20	0.06 – 0.11	α-pinene	0.16 – 0.21 (15 -60)	Pathak et al. (2007)
61 – 200[†]	0.22 – 0.30	0.12 – 0.15	α-pinene	0.22 (62)	Kristensen et al. (2017)
1.1– 550[†]	0.24 -0.48	0.007-0.06	limonene	0.26 (1.7)	Waring (2016)
0 - 100[†]	0 – 0.09[‼]	0 – 0.09	β-pinene	0.03-0.22 (7.2 - 100)	Griffin (1999)
0 -10[†]	0 – 0.01[‼]	0 – 0.01	β-caryophyllene	0.13 (1.8)	Chen et al. (2012)

[‼]indicates that no PRAM mechanism available yet i.e the yields are same as the MCM yields.

Table 2b. Mass yields for BVOCs ozonolysis at 293 K for different range of mass loadings using an OFR$^{\|}$ setup.

SOA mass loading (ppb)	MCM + PRAM mass yields range	MCM mass yields range	BVOC	Experimental yields	References
0-100$^{\|}$	0.07-0.25	0-0.13	α-pinene	0.2 (100)	Kang and Root (2007)
0-156$^{\|}$	0 – 0.02$^{\|}$	0 – 0.02	β-pinene	0.49 (156)	Kang and Root (2007)

337 $^{\|}$indicates that no PRAM mechanism available yet i.e the yields are same as the MCM yields.

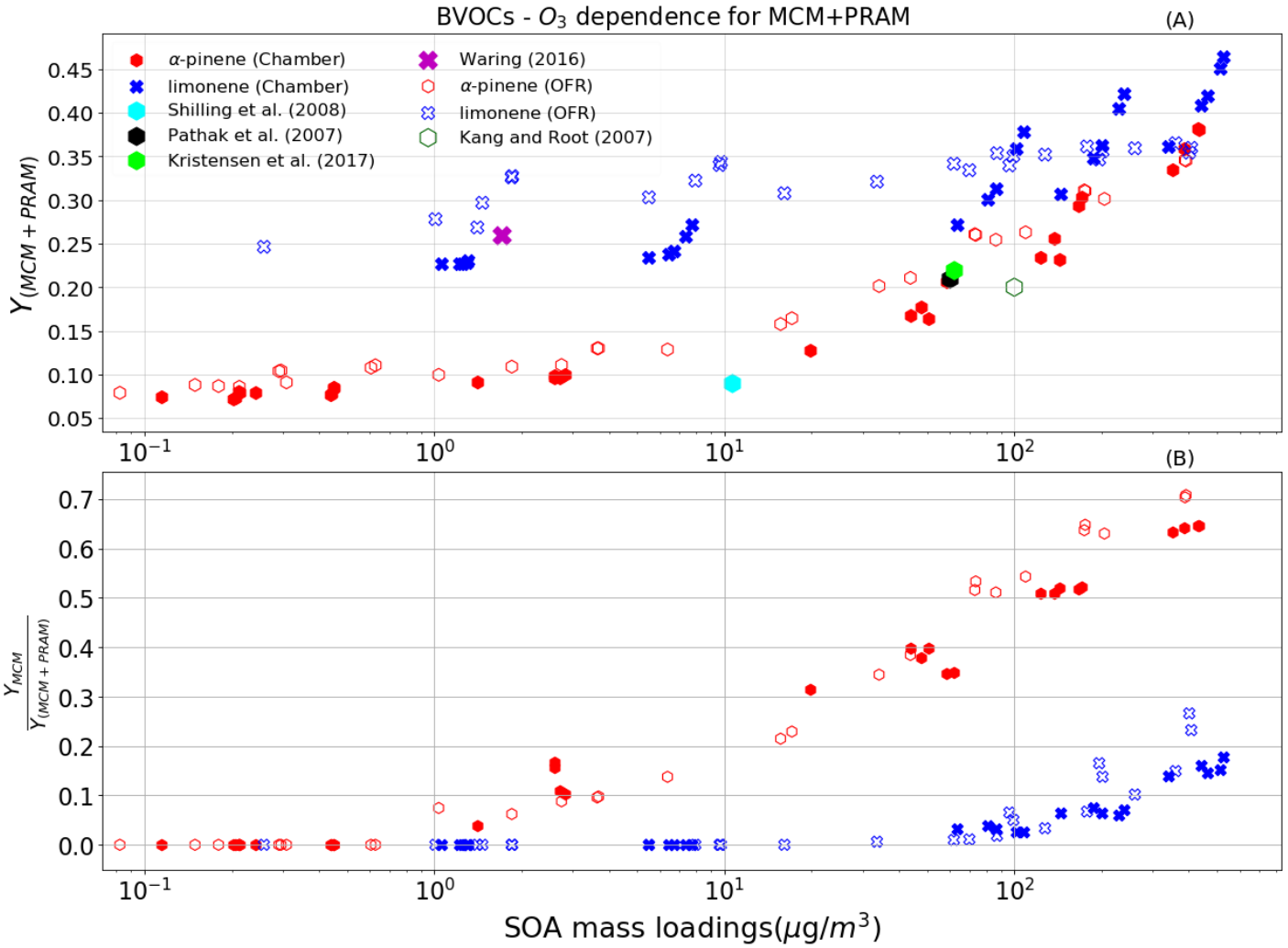

338 **Figure 1.** The mass yields from the ozonolysis of BVOCs α-pinene (red heptagon) and limonene (blue crosses) modelled after
339 chamber (filled symbols) and flow-tube settings (open symbols). The figure shows a comparison of SOA mass yields obtained from
340 simulations with MCM + PRAM (panel A) and ratio of yields from MCM and MCM+PRAM (panel B). Currently PRAM is

available for ozonolysis of limonene and α-pinene. The clumps are a result of SOA mass yields for the oxidation of specific oxidant concentration with varying BVOC concentration

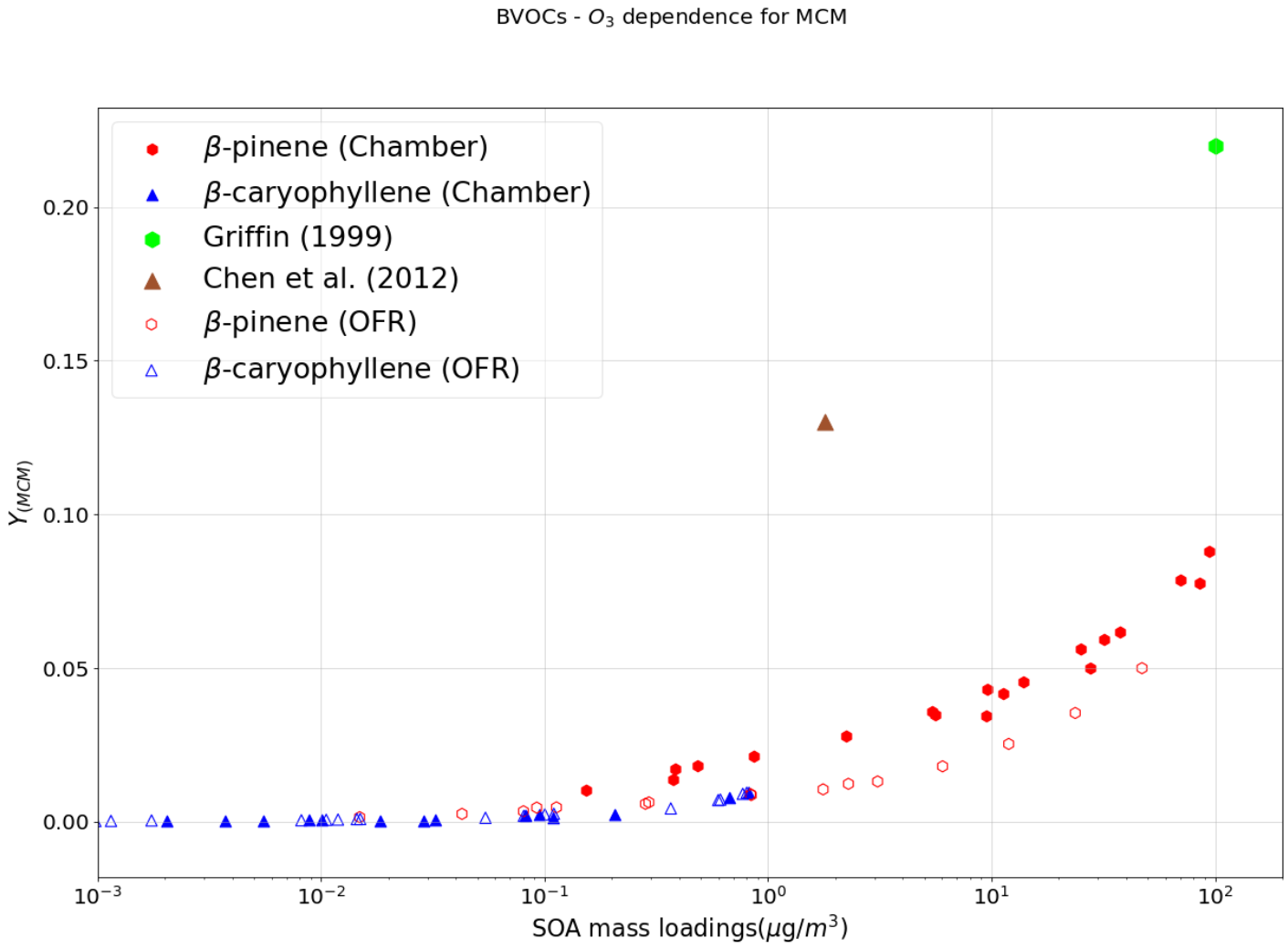

Figure 2. The mass yields from the ozonolysis of BVOCs β-pinene and β-caryophyllene modelled after chamber (filled symbols) and flow-tube (open symbols) settings. The figure shows a comparison of SOA mass yields obtained from simulations with only MCM as currently there is no PRAM available for these compounds. The experimental values are provided for comparison.

3.2 BVOCs – OH chamber and flow-tube simulations

The mass yields obtained by MCM+PRAM for α-pinene – OH oxidation are close to the measured values (Kristensen et al., 2017), while using only MCM under-predicts the mass yields (Figure 3 , panel A and B, and Table 3). The maximum SOA mass yield for OH oxidation of α-pinene is lower than the yield from ozonolysis which is suspected to arise due to the formation of more volatile oxidation products produced during OH oxidation (Bonn and Moortgat, 2002; Kristensen et al., 2014). The OH oxidation of β-pinene results in mass yields similar to the measurements obtained by Lee et al. (2006b) for similar mass loadings.

354 The β-pinene SOA yields are comparatively well represented by MCM+PRAM in comparison to the
355 standalone MCM. On the other hand, the limonene mass yields are under-predicted by MCM+PRAM for
356 similar mass loadings. Yields for limonene SOA mass loadings of 350 μg m^{-3} are around 0.31 which is lower
357 than the experimental values of 0.58, measured by Lee et al. (2006b).

358 For β-caryophyllene, the modeled values are in good agreement with experimental measured yields in
359 the range of mass loadings provided by Griffin (1999) and Tasoglou and Pandis (2015). Currently there are no
360 experiments providing HOM yields from OH oxidation of β-caryophyllene, and hence, those species are not
361 included in PRAM. The simulation results for yields from OH oxidation of β-caryophyllene, indicate that the
362 MCM scheme is able to reproduce the experimental values (Fig. 4). Only MCM was used for modeling the
363 mass yields for OH oxidation of isoprene due to current lack of PRAM mechanism for isoprene. The mass
364 yields derived from OH oxidation of isoprene vary from 0.01 - 0.31 covering a range of mass loadings from
365 0.003 - 132 μg m^{-3}. At low mass loadings < 10 μg m^{-3} the maximum yield obtained is ~0.06, which is a factor
366 of 3 greater than the experimental results obtained by (Lee et al., 2006b) where they measured yield of 0.02.
367 The mass yields are in good agreement with the experimental results from Liu et al. (2016), wherein they
368 measured a yield of 0.13 for 22 μg m^{-3} (Table 3).

369 The OFR simulations results for the OH oxidation of BVOCs with an equivalent exposure range from
370 2.0 x 10^{10} – 2.0 x 10^{12} molecules cm^{-3} s, is shown in Fig. 3. Our yields for α-pinene agree well with the yields
371 obtained by Bruns et al. (2015) where they measured yield of ~0.3 for mass loading of ~300 μg m^{-3} at
372 equivalent OH exposures. Friedman and Farmer (2018) found mass yields of 0 - 0.086 for α-pinene
373 (ammonium sulfate seeded experiment), 0- 0.12 for β-pinene (no seed particles) and 0-0.04 for limonene (no
374 seed particles), by varying the OH exposures between 4.7 x 10^{10} – 7.4 x 10^{11} molecules cm^{-3} s. Our simulated
375 yields for OH oxidation of α-pinene, β-pinene and limonene suggest higher mass yields for α-pinene and
376 limonene at equivalent mass loadings, while mass yields for β-pinene are in good agreement with the
377 experimental yields. Friedman and Farmer (2018) suggest that the reason for this underestimation in mass
378 yields could arise due to the exclusion of large particle sizes in the experiments and propose that these yields
379 could represent lower bounds.

380 **Table 3.** Mass yields for OH oxidation of BVOCs at 293 K for different range of mass loadings using a
381 chamber[†] and OFR[‖] setup.

SOA mass loading (µg m^{-3})	**MCM + PRAM mass yields**	**MCM mass yields**	**BVOC**	**Experimental yields**	**References**
300†	0.28	0.25	β-pinene	0.31 (293)	Lee et al. (2006b)
350†	0.31	0.06 – 0.11	limonene	0.58 (394)	Lee et al. (2006b)
30	0.09	0.004	α-pinene	0.11 (30)	Kristensen et al., 2017
< 10† 20 – 80†	0.21‼ 0.3 – 0.7‼	0.21 0.3 – 0.7	β-caryophyllene	0.2 (8.8) 0.37 – 0.79 (17-82)	Tasoglou and Pandis (2015) Griffin (1999)
22† <10	0.1‼ 0.06‼	0.1 0.06	Isoprene	0.13 (22) 0.02 (9)	Liu et al. (2016) Lee et al. (2006b)
0-300‖	0.05 – 0.31	0 – 0.2	α-pinene	0 – 0.086 (0 -300) 0.3 (300)	Friedman and Farmer (2018) Bruns et al. (2015)
0-30‖	0-0.1	0-0.01	β-pinene	0 – 0.12 (30)	Friedman and Farmer (2018)
0-40‖	0.-0.19	0-0.17	limonene	0.0 – 0.04 (35)	Friedman and Farmer (2018)

‼indicates that no PRAM mechanism available yet i.e the yields are same as the MCM yields.

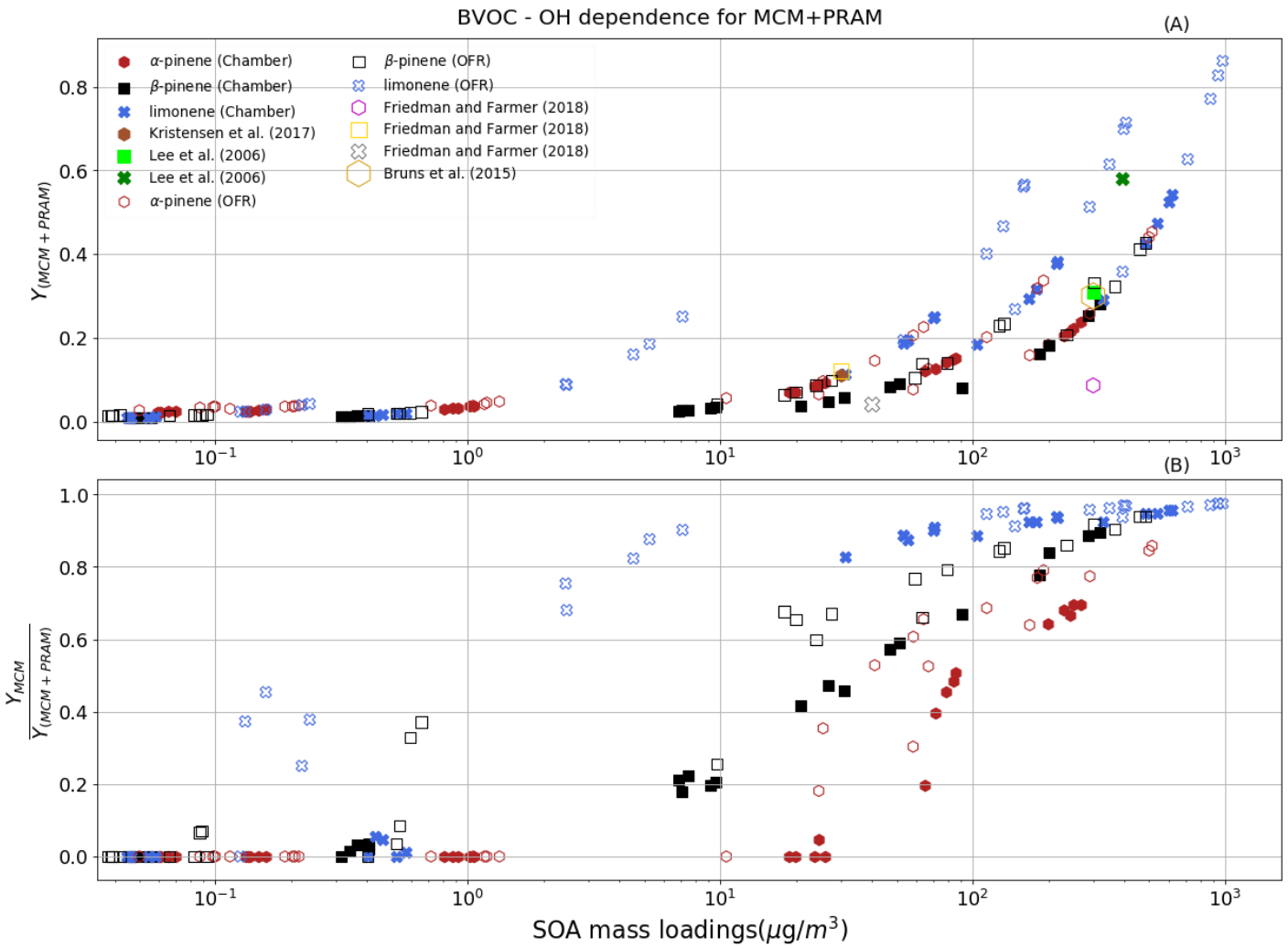

Figure 3. The mass yields from OH oxidation of BVOCs α-pinene (red heptagons), β-pinene (black squares) and limonene (blue crosses) modeled after chamber (filled symbols) and flow-tube settings (open symbols). The figure shows a comparison of SOA mass yields obtained from application of MCM+PRAM (panel A) and ratio of yields from MCM and couple MCM+PRAM (panel B). Currently PRAM is available for OH oxidation of limonene and α-pinene and β-pinene.

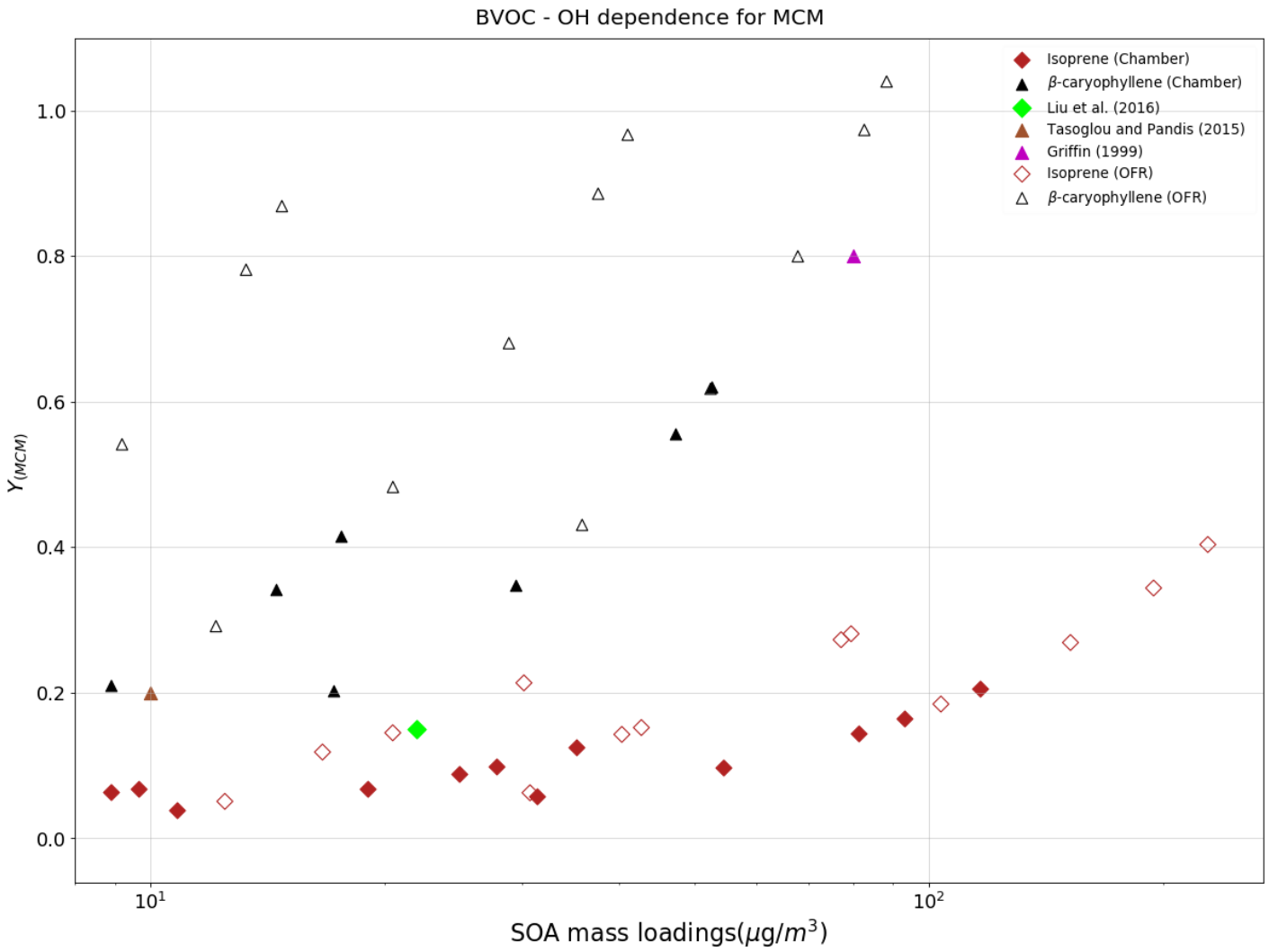

388 **Figure 4.** The mass yields from OH oxidation of BVOCs β-caryophyllene (black triangles) and isoprene (maroon diamonds)
389 modeled after chamber (filled symbols) and flow-tube settings (open symbols). The figure shows a comparison of SOA mass yields
390 obtained from application of MCM as currently there is no PRAM available for these compounds.

391 ### 3.3 BVOC – NO_3 chamber and OFR simulations

392 Figure 5. shows the yields derived from the oxidation of BVOCs by NO_3. Currently, as no PRAM is
393 available for NO_3 oxidation, Figure 5 represents SOA yields derived using MCM. Due to limited
394 experimental constraints, PRAM presently does not consider autoxidation of RO_2 formed from NO_3 oxidation
395 of VOCs,which could explain the huge discrepancy between the measured and simulated mass yields (Figure
396 5). The yields obtained for oxidation of α-pinene (0.002-0.007) by NO_3 are low in comparison to those
397 obtained by Nah et al. (2016), where they measured a yield of 0.036. Measured mass yields for limonene
398 oxidation by NO_3 resulting in mass yields between 0.25-0.4 (Fry et al., 2011), whereas we obtain negligible
399 (~0.0003) mass yields for the same.

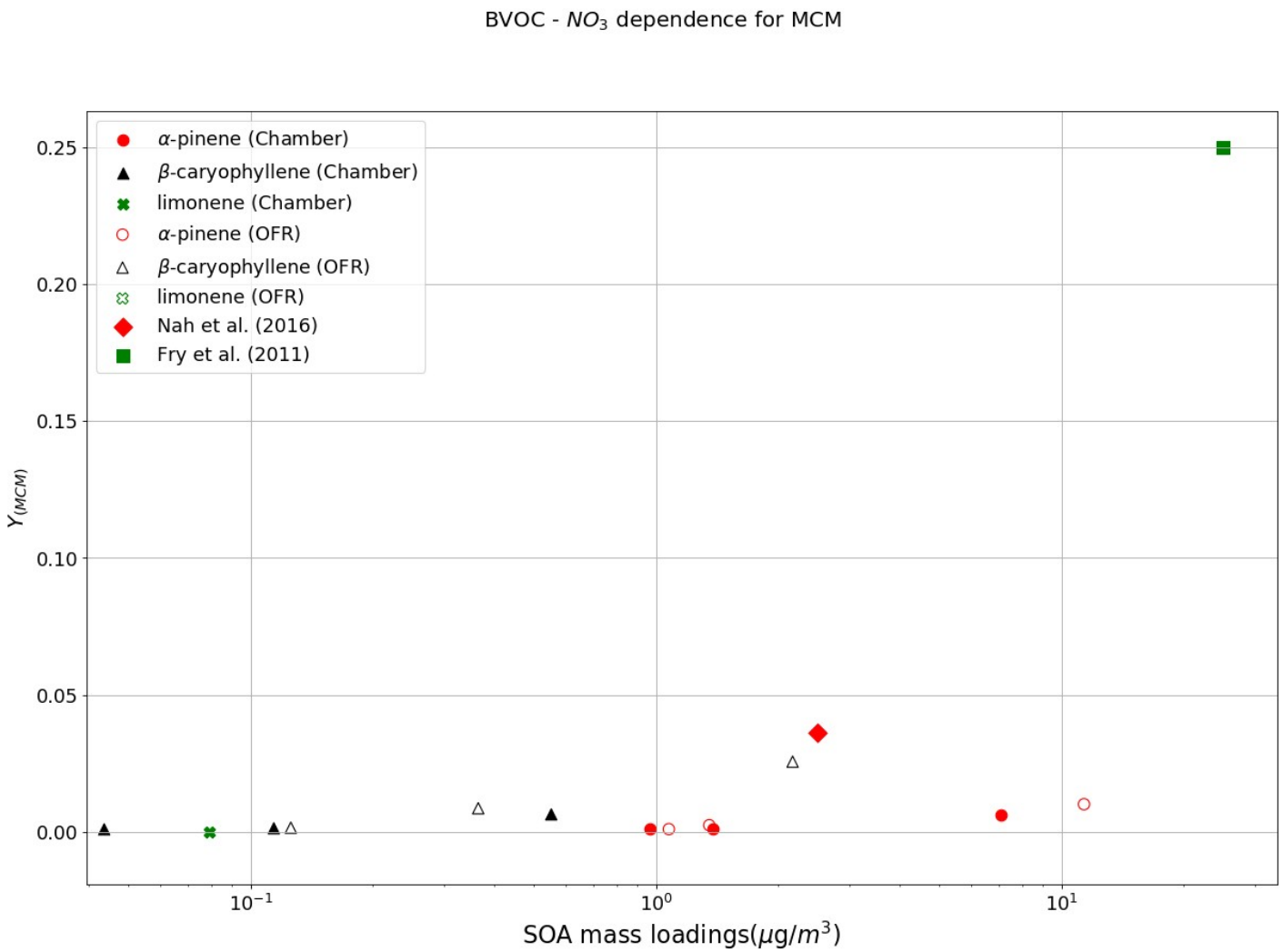

Figure 5. The mass yields from NO_3 oxidation of BVOCs modeled after chamber and flow-tube settings. The figure shows a comparison of SOA mass yields obtained from application of MCM. Appreciable mass yields were only obtained for α-pinene, limonene and β-caryophyllene.

3.4 NO_x dependence

Varying NO_x concentrations changes the fate of RO_2 radical formed during organic oxidations by altering HO_2/RO_2 ratio, thereby impacting the distribution of reaction products and aerosol formation (Presto et al., 2005; Zhao et al., 2018; Sarrafzadeh et al., 2016). We modeled the SOA mass yields for α-pinene - O_3 setup with varying NO_x concentrations (NO was varied whereas NO_2 was kept constant for all the runs), for initial α-pinene mixing ratios in the range 0.5 - 200 ppb (Fig. 6). A maximum SOA yield value of 0.55 is obtained for a combination of the lowest value of NO (0 ppb, red circles). As the NO concentrations increase from 0.2 ppb (blue squares) to 5 ppb (green inverted triangles) the yields begin to decrease, and this pattern is observable and valid for all concentration ranges of reacted precursor VOC. The NO_x dependence of α-pinene

ozonolysis is consistent with the findings of Draper et al. (2015) and Presto et al. (2005) wherein they observed a trend of decreasing SOA mass yields for α-pinene ozonolysis with increasing NO_x concentrations.

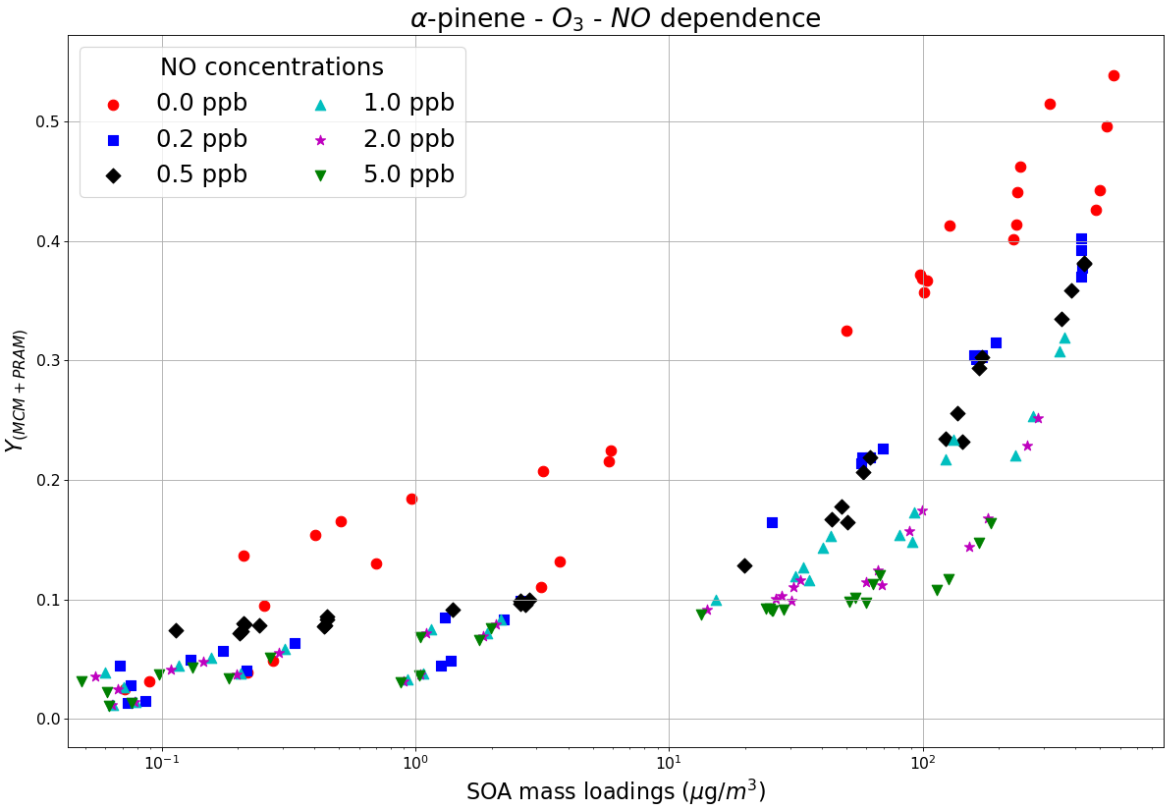

Figure 6. The SOA mass yields from O_3 oxidation of α-pinene modeled for different NO concentrations with the chamber setup. The model runs were performed using MCM+PRAM.

At low NO_x concentrations RO_2 radicals undergo rapid autoxidation until they react with HO_2 or RO_2 resulting in production of low volatility hydro-peroxide products (Sarrafzadeh et al., 2016), closed shell monomers or dimers (Ehn et al., 2014; Roldin et al., 2019), which increase SOA mass. This contrasts with high NO_x conditions where the RO_2+NO reactions dominate over reactions with HO_2 or RO_2, resulting in the formation of more volatile products such as aldehydes, ketones and organonitrates (Presto et al., 2005; Sarrafzadeh et al., 2016), and likely suppressing the autoxidation process leading to a decrease in SOA mass loadings (Ehn et al., 2014).

Figure 7 shows the absolute contributions to SOA mass loadings by PRAM and MCM compounds at two different O_3 concentrations of 4 and 100 ppb and varying NO concentrations. The figure shows that with an increase in NO concentrations more than 1 ppb the contribution of PRAM compounds to the particle phase

decreases at both 4 and 100 ppb of O_3 concentrations. In PRAM the RO_2 + NO reaction leads either to the formation of organonitrate HOM, closed shell monomers with carbonyl group or fragmentation products with higher volatility (Roldin et al., 2019). HOM Dimer formation is suppressed with increasing NO concentrations in PRAM (Roldin et al., 2019) which explains the lower contribution by PRAM compounds to SOA mass loadings with increasing NO. At NO concentrations <1ppb the PRAM contribution increases as, first generation RO_2 are capable of undergoing autoxidation forming highly oxygenated RO_2 which subsequently reacts with NO forming organic nitrates (Ehn et al., 2014). As NO concentrations exceed 1ppb the first generation RO_2 is scavenged by NO thereby reducing the concentration of organonitrate HOM (Ehn et al., 2014), possibly affecting SOA yields. The MCM contribution also decreases with increasing NO concentrations mostly due to the formation of more volatile organonitrates (Jenkin et al., 2019) .

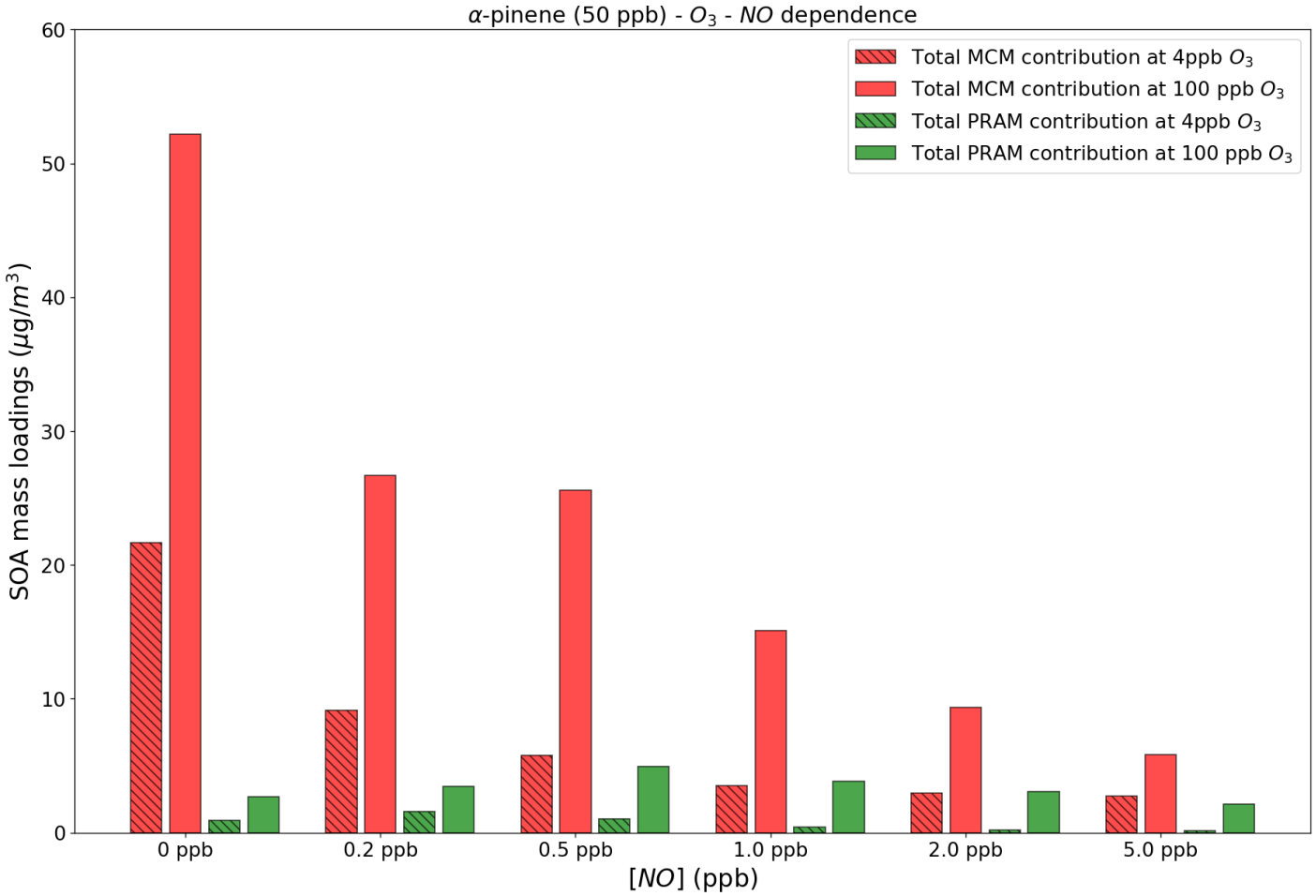

Figure 7. Contribution to the SOA mass loadings by total PRAM and MCM compounds at different NO levels and O_3 concentrations. For comparison we use 4 ppb and 100 ppb O_3 concentrations, respectively, at 50 ppb α-pinene.

3.5 Temperature dependence

The formation of SOA from α-pinene ozonolysis in the temperature range of 258.15 - 313.15 K was investigated in this study using MCM+PRAM. Strong dependence of SOA mass yield on temperature was reported by Saathoff and Naumann, (2009) wherein they measured the decreasing mass yields from 0.42 at 273.15 K to 0.09 to 313.15 K for SOA loadings of 53 and 92 μg m^{-3} respectively. Our results in Figure 8 show increasing SOA mass yields for α-pinene ozonolysis with decreasing temperature, which is attributed to the augmented condensation of oxidation products termed as semi volatile organic compounds (SVOC) (Kristensen et al., 2017) at lower temperatures.

For α-pinene maximum mass loading < 150 μg m^{-3} the mass yields reach a maximum value of 0.38 at temperatures as low as 258.15 K and decrease to 0.27 for a temperature of 293.15 K and to 0.1 for the temperature of 313.15 K. These yields are comparable to the results obtained by Kristensen et al. (2017) where they measured yields of 0.39 for 258.15 K and 0.22 for 293.15 K for mass loading <150 μg m^{-3}. The results show a weak dependence of SOA mass yields on temperatures in the range of 278.15 K - 313.15 K at low SOA mass loadings which become more pronounced as the mass loadings increase. At the lowest temperature of 258.15 K the mass yields are higher in comparison to other temperatures regardless the mass loadings. These results are in good agreement with the findings by Pathak et al. (2007) where they found a strong temperature dependence of SOA mass yields at lower temperature (0 – 15^{o} C), which decreases as the temperature increases. Furthermore, similar to the measurements made by Pathak et al. (2007), our simulations were able to reproduce the experimental findings that show no appreciable differences in the SOA mass yields for loadings below 1 μg m^{-3} (initial mixing ratio of 1 ppb) for temperatures > 273.15 K.

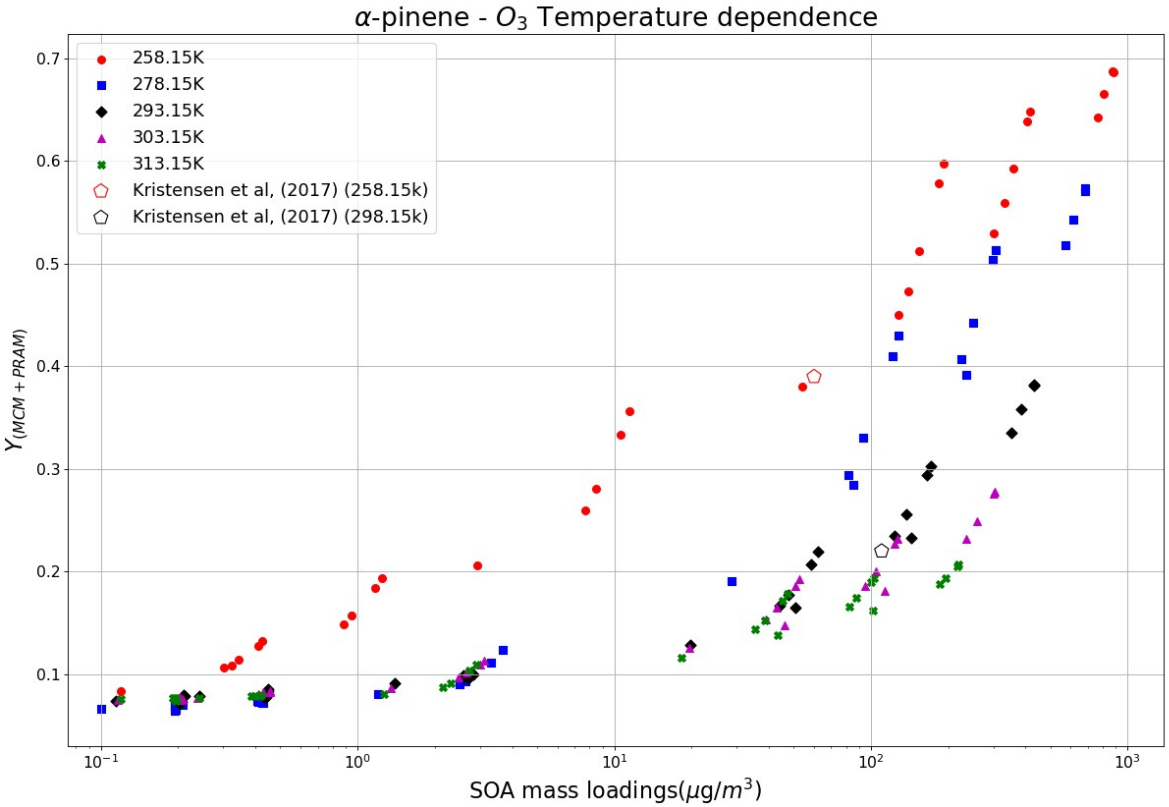

460 **Figure 8**. Temperature dependence of SOA mass yields at different temperatures using the MCM+PRAM. The open pentagons
461 represent measurement data from Kristensen et al. (2017) at 258.15 K and 298.15 K.

462 Figure 9 shows the volatility distribution of α-pinene ozonolysis derived SOA at different
463 temperatures. The saturation vapor pressure limits for defining extremely low volatility (ELVOCs - grey
464 shaded), low volatility (LVOCs - red shaded), semi volatile (SVOCs - green shaded) and intermediate
465 volatility (IVOCs - cyan shaded) organic compounds used in the Volatility basis set (VBS) are set according
466 to the values suggested in Donahue et al. (2012). In this work, we categorize compounds (ELVOCs, LVOCs,
467 SVOCs and IVOCs) based on effective saturation vapor pressures (C*) in the range of $\{10^{-5}$ to $10^{3}\}$ µg m^{-3}
468 and temperature of 298 K (Donahue et al., 2009). At the lowest temperature of 258.15 K, the SVOCs
469 contribution to the particle phase is dominant in comparison to LVOCs and ELVOCs, a trend which is
470 subsequently reversed as the temperatures are increased. At 293.15 K a majority of SVOCs and IVOCs are in
471 the gas phase while the contribution of LVOCs and ELVOCs to particle phases increases. These results are in
472 good agreement with observations made by Kristensen et al. (2017) wherein they observed an increasing
473 contribution of SVOCs at sub-zero temperatures of 258.15 K, which decrease the fraction of SOA formed

474 from ELVOCs. Again, it should be noted that the temperature dependence of peroxy radical autoxidation
475 product formation still needs further validation based on recent experiments (e.g. Quéléver et al., 2019).
476

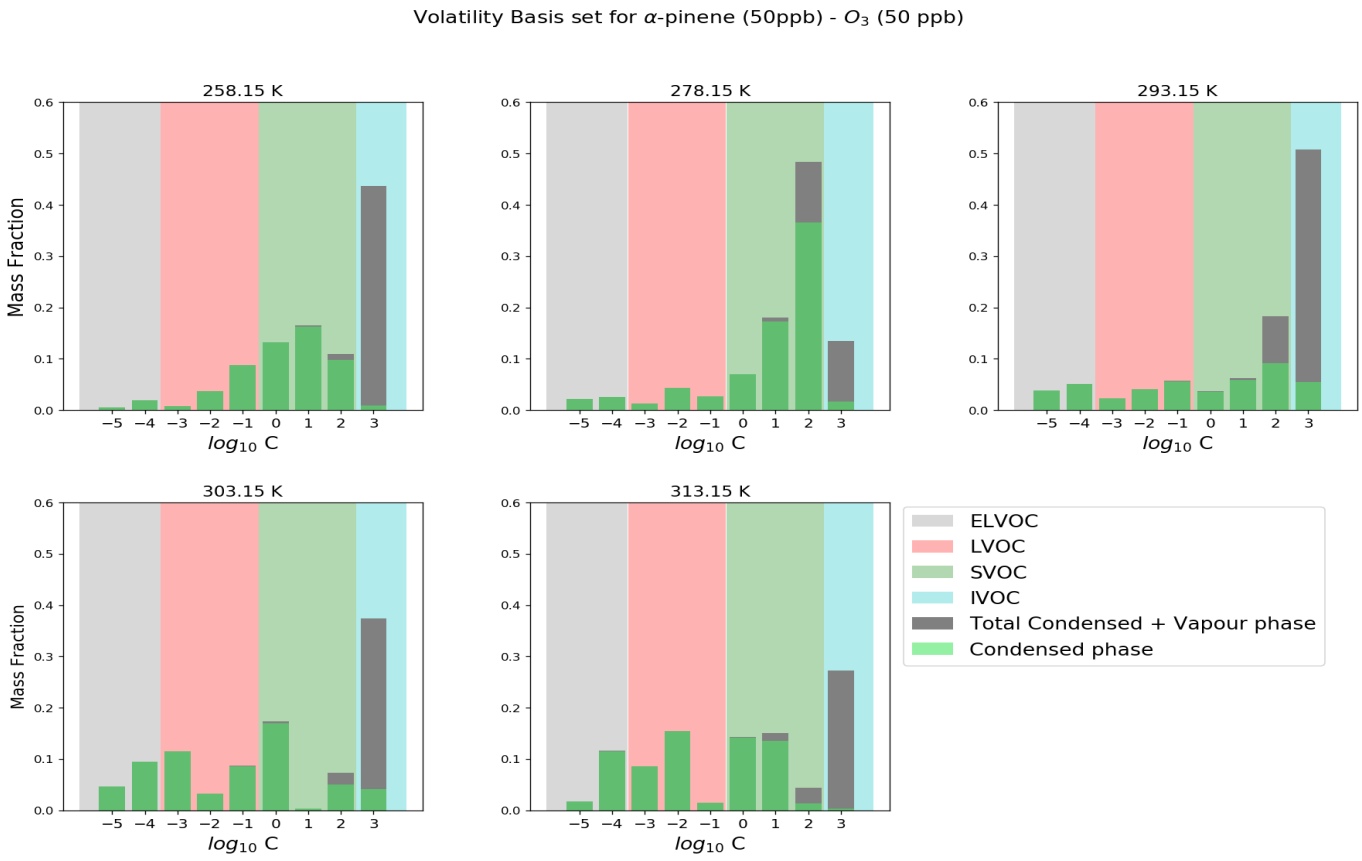

477 **Figure 9**. Modeled volatility distribution of SOA at different temperatures. The volatility bins span a range of effective saturation
478 vapor pressures C = C* = $\{10^{-5}$ to $10^{3}\}$ µg m^{-3}. The VBS distribution is based on a reference temperature of 298 K.

479 ## 3.6 Composition

480 MCM+PRAM can be used to narrow down and compile a list of compounds playing a pivotal role in
481 contributing to SOA mass loadings and, also compare the relative importance of implementing PRAM
482 alongside the MCM. Figure 10 shows the most important compounds from both the MCM and PRAM that
483 together contribute to more than 95% of α-pinene ozonolysis SOA mass loading at 293.15 K.

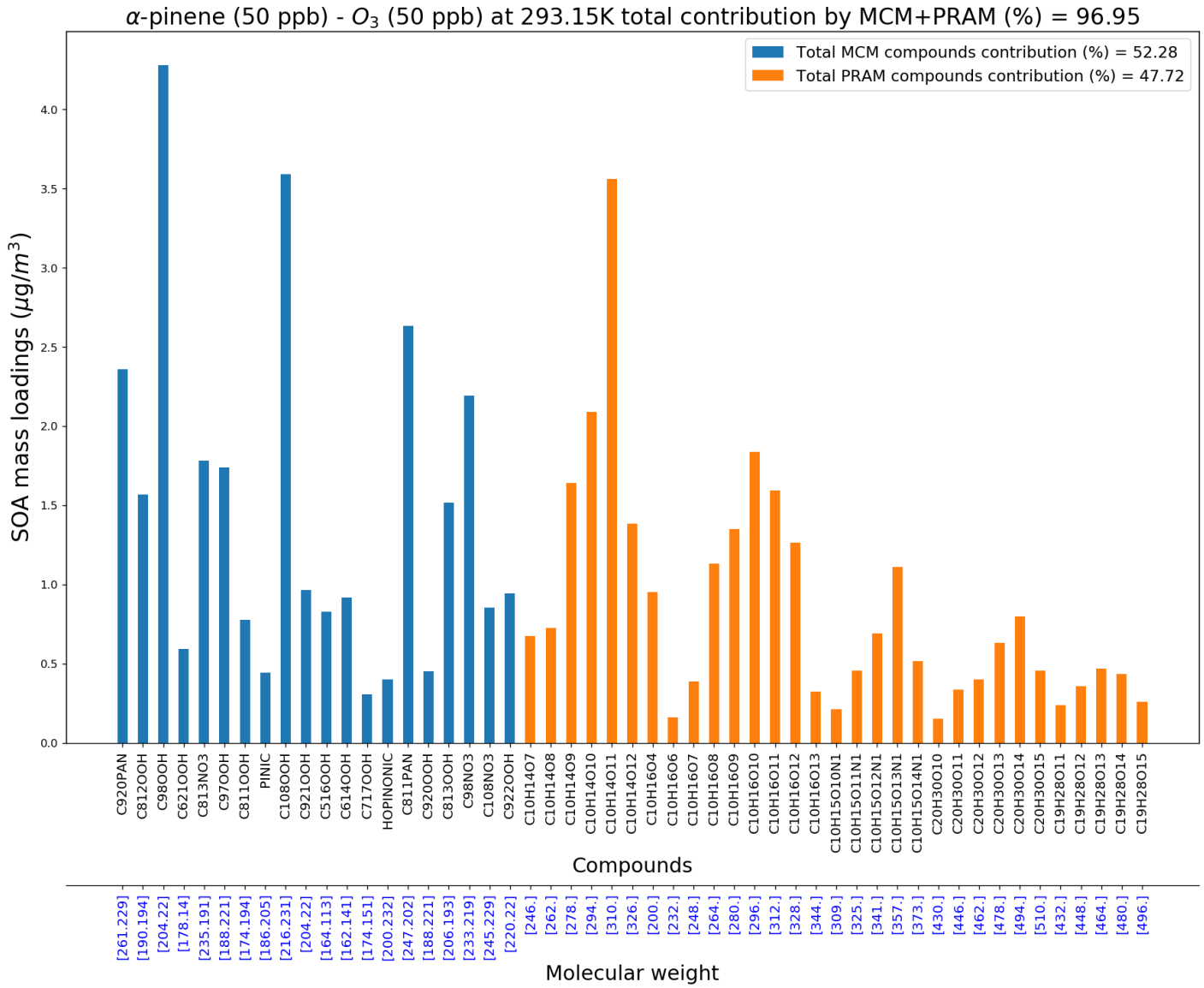

Figure 10. MCM and PRAM Compounds contributing to > 95 % of SOA mass at 293 K and 50ppb O_3 and α-pinene concentrations.

Figure 10 shows that contribution to SOA mass loadings by PRAM compounds is ~48 % (of 97 %) while MCM compounds contribute ~52 % (of 97%). On lowering the temperature to 258K the relative contributions of PRAM drop to 15 % (of ~99 %), while MCM dominates by contributing ~85 % (of ~99 %) respectively (Figure S3a). The contribution of PRAM increases to ~64 % (of ~97 %) and MCM contribution drops to 36 % (of ~97 %) at 313 K (Figure S3b). These results reflect the importance of PRAM as its contribution plays an increasingly dominant role with increasing temperatures and highlights the crucial few compounds that contribute to maximum SOA mass loadings for α-pinene ozonolysis. The list of abundant compounds which together add up to contribute more than 95 % of SOA mass loadings at 258 K, 293 K and 313 K are presented in the supplement Table 1s (a, b & c). At 258 K MCM compounds namely pinonic acid ($C_{10}H_{16}O_3$, 4.4 %),

C920PAN ($C_{10}H_{15}NO_7$, 9.3 %), C108NO3 ($C_{10}H_{15}NO_6$, 8.9 %), C811PAN ($C_9H_{13}NO_7$, 10.1 %), C717NO3 ($C_7H_9NO_6$, 11.3 %) contribute significantly to the total SOA mass loadings while PRAM compounds such as $C_{10}H_{14}O_7$ (0.88 %), $C_{10}H_{16}O_4$ (1.3 %), $C_{10}H_{16}O_6$ (1.13 %) contribute significantly less. An increase in temperature to 293 K results in an overall increase in contribution by PRAM compounds, with $C_{10}H_{14}O_{10}$ (3.6 %), $C_{10}H_{14}O_{11}$ (6.2 %), $C_{10}H_{16}O_{10}$ (3.2 %) playing an important role in contributing to the SOA mass loadings. This trend of relative increase in the contribution by PRAM compounds over MCM compounds to SOA mass loadings is also evident as the temperatures are further increased to 313 K, where the PRAM compounds $C_{10}H_{14}O_{11}$ (18.3 %), $C_{10}H_{14}O_{12}$ (6 %) and $C_{10}H_{16}O_{12}$ (6.6 %) play a dominant role in increasing SOA mass loadings.

4. Conclusions

We simulated SOA mass yields derived from the oxidation of various BVOCs (isoprene, α-pinene, β-pinene, limonene and β-caryophyllene), by the oxidants O_3, OH and NO_3 using the zero-dimensional model MALTE-Box. The gas phase chemistry was simulated using the MCM in conjunction with PRAM. The aim was to verify the efficacy of MCM+PRAM in simulating the SOA mass yields. Additional simulations were performed to test the MCM+PRAM under varying temperature and NO concentrations. A few important compounds playing a major role in increasing the SOA mass yields for α-pinene ozonolysis at different temperatures are also highlighted.

The simulations were designed to resemble ideal smog chambers experiments and experiments in oxidative flow reactors (OFR). No interactions between the gas phase and chamber walls were considered during the simulations. For the smog chamber setting, the standalone MCM generally under-predicts the mass yields obtained by the ozonolysis and OH oxidation of BVOCs. In contrast, the yields derived using MCM+PRAM for the smog chamber setup is in good agreement with the experimental results. For an idealized OFR setup, MCM+PRAM yields are in good agreement with experimental yields, while again the MCM under-predicts the SOA yields. The relative contribution of HOM monomers and dimers to the particle phase in OFR simulations is low when compared to the chamber simulations. This is due to higher RO_2 concentrations in OFR leading to termination of peroxy radical autoxidation, thereby affecting SOA yields. This needs to be considered when applying yields based on OFR simulations in regional or global chemical transport models

The model does not simulate appreciable SOA mass yields for oxidation of BVOCs with NO_3, as PRAM currently does not consider autoxidation of RO_2 formed from NO_3 oxidation of VOCs. This underlines the need for developing a NO_3 oxidation scheme which can better constrain and predict SOA mass yields. In

accordance to the previous studies, the simulated SOA yields tend to decrease at higher temperatures. The PRAM contribution to mass yields at low temperatures (258.15 K) is ~14 %, which is substantially lower than that of MCM (~86 %). As the temperature is increased to 313.15 K, the contribution of PRAM to SOA mass yields begins to dominate over MCM. This most likely is due to MCM producing more SVOCs (compounds classified as SVOCs at 298 K), which show stronger contribution to particle phase at lower temperatures, due to decrease in saturation vapor pressures with temperature. It should be noted that the present temperature dependency of mass yields using PRAM are a first, and currently the best estimate in understanding the influence of temperature on the peroxy radical autoxidation formation. The simulated SOA yields with varying NO concentrations agree well with experimental results, i.e. SOA yields decrease with increasing NO concentrations due to the formation of more volatile compounds such as organonitrates and ketones.

Using PRAM coupled with MCM helps us bridge the gap in understanding the role and contribution of peroxy radical autoxidation to SOA formation. The variation of SOA yields for temperature and NO concentrations, indicates the limitations of global and regional models in predicting e.g. cloud condensation nuclei (CCN) effects using fixed SOA yields. The good agreement of modeled and experimental yields from smog chambers, could further help us parameterize the SOA yields, that could be applied at a global and regional model scale, to more accurately predict the direct and indirect impact of aerosol particles on e.g. radiation balance by aerosol scattering/absorption and CCN concentrations. Furthermore, implementation of a condensed PRAM version to regional and global models has been tested but still need further validation (Roldin et al., 2019).

Data availability

The complete PRAM mechanism written in a format compatible with the Kinetic PreProcessor (KPP) together with all species information can also be downloaded from https://doi.org/10.1594/PANGAEA.905102

Author Contributions

CX and MB served as the chief authors and editors of the paper. CX was performing the model simulations. The study was designed by CX, MB and PR. All other co-authors contributed to the analysis and writing of the paper.

Acknowledgements

The presented research has been funded by the Academy of Finland (Center of Excellence in Atmospheric Sciences) grant no. 4100104 and the Swedish Research Council FORMAS, project no. 2018-01745. We would also like to acknowledge the invaluable contribution of computational resources from CSC – IT Center for Science, Finland.

References

Ahlberg, E., Eriksson, A., Brune, W. H., Roldin, P. and Svenningsson, B.: Effect of salt seed particle surface area, composition and phase on secondary organic aerosol mass yields in oxidation flow reactors, Atmos. Chem. Phys., 19(4), 2701–2712, doi:10.5194/acp-19-2701-2019, 2019.

Berndt, T., Richters, S., Jokinen, T., Hyttinen, N., Kurtén, T., Otkjær, R. V., Kjaergaard, H. G., Stratmann, F., Herrmann, H., Sipilä, M., Kulmala, M. and Ehn, M.: Hydroxyl radical-induced formation of highly oxidized organic compounds, Nat. Commun., 7(May), doi:10.1038/ncomms13677, 2016.

Bianchi, F., Garmash, O., He, X., Yan, C., Iyer, S., Rosendahl, I., Xu, Z., Rissanen, M. P., Riva, M., Taipale, R., Sarnela, N., Petäjä, T., Worsnop, D. R., Kulmala, M., Ehn, M. and Junninen, H.: The role of highly oxygenated molecules (HOMs) in determining the composition of ambient ions in the boreal forest, Atmos. Chem. Phys., 17(22), 13819–13831, doi:10.5194/acp-17-13819-2017, 2017.

Bianchi, F., Kurtén, T., Riva, M., Mohr, C., Rissanen, M. P., Roldin, P., Berndt, T., Crounse, J. D., Wennberg, P. O., Mentel, T. F., Wildt, J., Junninen, H., Jokinen, T., Kulmala, M., Worsnop, D. R., Thornton, J. A., Donahue, N., Kjaergaard, H. G. and Ehn, M.: Highly Oxygenated Organic Molecules (HOM) from Gas-Phase Autoxidation Involving Peroxy Radicals: A Key Contributor to Atmospheric Aerosol, Chem. Rev., doi:10.1021/acs.chemrev.8b00395, 2019.

Bonn, B. and Moortgat, G. K.: New particle formation during α- and β-pinene oxidation by O3, OH and NO3, and the influence of water vapour: Particle size distribution studies, Atmos. Chem. Phys., 2(3), 183–196, doi:10.5194/acp-2-183-2002, 2002.

Boy, M., Hellmuth, O., Korhonen, H., Nilsson, E. D., Revelle, D., Turnipseed, A., Arnold, F. and Kulmala, M.: MALTE - Model to predict new aerosol formation in the lower troposphere, Atmos. Chem. Phys., 6(12), 4499–4517, doi:10.5194/acp-6-4499-2006, 2006.

Bruns, E. A., El Haddad, I., Keller, A., Klein, F., Kumar, N. K., Pieber, S. M., Corbin, J. C., Slowik, J. G., Brune, W. H., Baltensperger, U. and Prévôt, A. S. H.: Inter-comparison of laboratory smog chamber and flow reactor systems on organic aerosol yield and composition, Atmos. Meas. Tech., 8(6), 2315–2332, doi:10.5194/amt-8-2315-2015, 2015.

Chen, Q., Li, Y. L., McKinney, K. A., Kuwata, M. and Martin, S. T.: Particle mass yield from β-caryophyllene ozonolysis, Atmos. Chem. Phys., 12(7), 3165–3179, doi:10.5194/acp-12-3165-2012, 2012.

Crounse, J. D. and Nielsen, L. B.: Autoxidation of Organic Compounds in the Atmosphere, J. Phys. Chem. Lett., 24(4), 3513–3520, doi:10.1021/jz4019207, 2013.

Damian, V., Sandu, A., Damian, M., Potra, F. and Carmichael, G. R.: The kinetic preprocessor KPP - A software environment for solving chemical kinetics, Comput. Chem. Eng., 26(11), 1567–1579, doi:10.1016/S0098-1354(02)00128-X, 2002.

Donahue, N. M., Robinson, A. L., Stanier, C. O. and Pandis, S. N.: Coupled Partitioning, Dilution, and Chemical Aging of Semivolatile Organics, Environ. Sci. Technol., 40(8), 2635–2643, doi:10.1021/es052297c, 2006.

Donahue, N. M., Robinson, A. L. and Pandis, S. N.: Atmospheric organic particulate matter: From smoke to secondary organic aerosol, Atmos. Environ., 43(1), 94–106, doi:https://doi.org/10.1016/j.atmosenv.2008.09.055, 2009.

Donahue, N. M., Kroll, J. H., Pandis, S. N. and Robinson, A. L.: A two-dimensional volatility basis set-Part 2: Diagnostics of organic-aerosol evolution, Atmos. Chem. Phys., 12(2), 615–634, doi:10.5194/acp-12-615-2012, 2012.

Draper, D. C., Farmer, D. K., Desyaterik, Y. and Fry, J. L.: A qualitative comparison of secondary organic aerosol yields and composition from ozonolysis of monoterpenes at varying concentrations of NO2, Atmos. Chem. Phys., 15(21), 12267–12281, doi:10.5194/acp-15-12267-2015, 2015.

Ehn, M., Kleist, E., Junninen, H., Petäjä, T., Lönn, G., Schobesberger, S., Dal Maso, M., Trimborn, A., Kulmala, M., Worsnop, D. R., Wahner, A., Wildt, J. and Mentel, T. F.: Gas phase formation of extremely oxidized pinene reaction products in chamber and ambient air, Atmos. Chem. Phys., 12(11), 5113–5127, doi:10.5194/acp-12-5113-2012, 2012.

Ehn, M., Thornton, J. A., Kleist, E., Sipilä, M., Junninen, H., Pullinen, I., Springer, M., Rubach, F., Tillmann, R., Lee, B., Lopez-Hilfiker, F., Andres, S., Acir, I. H., Rissanen, M., Jokinen, T., Schobesberger, S., Kangasluoma, J., Kontkanen, J., Nieminen, T., Kurtén, T., Nielsen, L. B., Jørgensen, S., Kjaergaard, H. G., Canagaratna, M., Maso, M. D., Berndt, T., Petäjä, T., Wahner, A., Kerminen, V. M., Kulmala, M., Worsnop, D. R., Wildt, J. and Mentel, T. F.: A large source of low-volatility secondary organic aerosol, Nature, 506(7489), 476–479, doi:10.1038/nature13032, 2014.

Friedman, B. and Farmer, D. K.: SOA and gas phase organic acid yields from the sequential photooxidation of seven monoterpenes, Atmos. Environ., 187(January), 335–345, doi:10.1016/j.atmosenv.2018.06.003, 2018.

Fry, J. L., Kiendler-Scharr, A., Rollins, A. W., Brauers, T., Brown, S. S., Dorn, H. P., Dubé, W. P., Fuchs, H., Mensah, A., Rohrer, F., Tillmann, R., Wahner, A., Wooldridge, P. J. and Cohen, R. C.: SOA from limonene: Role of NO 3 in its generation and degradation, Atmos. Chem. Phys., 11(8), 3879–3894, doi:10.5194/acp-11-3879-2011, 2011.

Glasius, M. and Goldstein, A. H.: Recent Discoveries and Future Challenges in Atmospheric Organic Chemistry, Environ. Sci. Technol., 50(6), 2754–2764, doi:10.1021/acs.est.5b05105, 2016.

Griffin, R. J.: Organic aerosol formation from the oxidation of biogenic hydrocarbons, , 104(D3), 3555–3567, 1999.

Guenther, A., Baugh, B., Brasseur, G., Greenberg, J., Harley, P., Klinger, L., Serca, D., and Vierling, L.: Isoprene emission estimates and uncertainties for the Central African EXPRESSO study domain, J. Geophys. Res. Atmos., 104(D23), 30625–30639, doi:10.1029/1999JD900391, 1999.

Guenther, A., Nicholas Hewitt, C., David, E., Fall, R., Chris, G., Tom, G., Peter, H., Klinger, L., Manuel, L., Mckay, W. A., Tom, P., Scholes, B., Steinbrecher, R., Tallamraju, R., Taylor, J. and Zimmerman, P.: A global model of natural volatile organic compound emissions s Raja the balance Triangle changes in the atmospheric accumulation rates of greenhouse Triangle Several inventories of natural and Exposure Assessment global scales have been two classes Fores, J. Geophys. Res., 100(94), 8873–8892, doi:doi:10.1029/94JD02950, 1995.

Guenther, A., Geron, C., Pierce, T., Lamb, B., Harley, P. and Fall, R.: Natural emissions of non-methane volatile organic compounds, carbon monoxide, and oxides of nitrogen from North America, Atmos. Environ., 34(12–14), 2205–2230, doi:10.1016/S1352-2310(99)00465-3, 2000.

Hao, L. Q., Romakkaniemi, S., Yli-Pirilä, P., Joutsensaari, J., Kortelainen, A., Kroll, J. H., Miettinen, P., Vaattovaara, P., Tiitta, P., Jaatinen, A., Kajos, M. K., Holopainen, J. K., Heijari, J., Rinne, J., Kulmala, M., Worsnop, D. R., Smith, J. N. and Laaksonen, A.: Mass yields of secondary organic aerosols from the

oxidation of α-pinene and real plant emissions, Atmos. Chem. Phys., 11(4), 1367–1378, doi:10.5194/acp-11-1367-2011, 2011.

Henry, K. M., Lohaus, T. and Donahue, N. M.: Organic Aerosol Yields from α-Pinene Oxidation: Bridging the Gap between First-Generation Yields and Aging Chemistry, Environ. Sci. Technol., 46(22), 12347–12354, doi:10.1021/es302060y, 2012.

Jacobson, M. Z.: Numerical techniques to solve condensational and dissolutional growth equations when growth is coupled to reversible reactions, Aerosol Sci. Technol., 27(4), 491–498, doi:10.1080/02786829708965489, 1997.

Jenkin, M. E., Saunders, S. M. and Pilling, M. J.: The tropospheric degradation of volatile organic compounds: A protocol for mechanism development, Atmos. Environ., 31(1), 81–104, doi:10.1016/S1352-2310(96)00105-7, 1997.

Jenkin, M. E., Young, J. C. and Rickard, A. R.: The MCM v3.3.1 degradation scheme for isoprene, Atmos. Chem. Phys., 15(20), 11433–11459, doi:10.5194/acp-15-11433-2015, 2015.

Jenkin, M. E., Wyche, K. P., Evans, C. J., Carr, T., Monks, P. S., Alfarra, M. R., Barley, M. H., McFiggans, G. B., Young, J. C. and Rickard, A. R.: Development and chamber evaluation of the MCM v3.2 degradation scheme for β-caryophyllene, Atmos. Chem. Phys., 12(11), 5275–5308, doi:10.5194/acp-12-5275-2012, 2012.

Jenkin, M. E., Valorso, R., Aumont, B., Rickard, A. R., Cnrs, U. M. R., Créteil, U. P. and Paris, U. De: Estimation of rate coefficients and branching ratios for reactions of organic peroxy radicals for use in automated mechanism construction, , (2), 7691–7717, 2019.

Jokinen, T., Berndt, T., Makkonen, R., Kerminen, V.-M., Junninen, H., Paasonen, P., Stratmann, F., Herrmann, H., Guenther, A. B., Worsnop, D. R., Kulmala, M., Ehn, M. and Sipilä, M.: Production of extremely low volatile organic compounds from biogenic emissions: Measured yields and atmospheric implications, Proc. Natl. Acad. Sci., 112(23), 7123–7128, doi:10.1073/pnas.1423977112, 2015.

Kanakidou, M., Seinfeld, J. H., Pandis, S. N., Barnes, I., Dentener, F. J., Facchini, M. C. and Dingenen, R. Van: Organic aerosol and global climate modelling: a review, , 1053–1123, 2005.

Kang, E. and Root, M. J.: Introducing the concept of Potential Aerosol Mass (PAM), Atmos. Chem. Phys., (7), 5727–5744

Keywood, M. D., Varutbangkul, V., Bahreini, R., Flagan, R. C. and Seinfeld, J. H.: Secondary organic aerosol formation from the ozonolysis of cycloalkenes and related compounds, Environ. Sci. Technol., 38(15), 4157–4164, doi:10.1021/es035363o, 2004.

Korhonen, H., Lehtinen, K. E. J. and Kulmala, M.: Atmospheric Chemistry and Physics Multicomponent aerosol dynamics model UHMA: model development and validation, Atmos. Chem. Phys, 4, 757–771, doi:10.1002/erv.2305, 2004.

Kristensen, K., Cui, T., Zhang, H., Gold, A., Glasius, M. and Surratt, J. D.: Dimers in α-pinene secondary organic aerosol: Effect of hydroxyl radical, ozone, relative humidity and aerosol acidity, Atmos. Chem. Phys., 14(8), 4201–4218, doi:10.5194/acp-14-4201-2014, 2014.

Kristensen, K., Jensen, L. N., Glasius, M. and Bilde, M.: The effect of sub-zero temperature on the formation and composition of secondary organic aerosol from ozonolysis of alpha-pinene, Environ. Sci. Process. Impacts, 19(10), 1220–1234, doi:10.1039/c7em00231a, 2017.

678 Kroll, J. H., Ng, N. L., Murphy, S. M., Flagan, R. C. and Seinfeld, J. H.: Secondary organic aerosol formation
679 from isoprene photooxidation under high-NOxconditions, Geophys. Res. Lett., 32(18), 1–4,
680 doi:10.1029/2005GL023637, 2005.

681 Lambe, A. T., Onasch, T. B., Massoli, P., Croasdale, D. R., Wright, J. P., Ahern, A. T., Williams, L. R.,
682 Worsnop, D. R., Brune, W. H. and Davidovits, P.: Laboratory studies of the chemical composition and cloud
683 condensation nuclei (CCN) activity of secondary organic aerosol (SOA) and oxidized primary organic aerosol
684 (OPOA), Atmos. Chem. Phys., 11(17), 8913–8928, doi:10.5194/acp-11-8913-2011, 2011.

685 Lambe, A. T., Chhabra, P. S., Onasch, T. B., Brune, W. H., Hunter, J. F., Kroll, J. H., Cummings, M. J.,
686 Brogan, J. F., Parmar, Y., Worsnop, D. R., Kolb, C. E. and Davidovits, P.: Effect of oxidant concentration,
687 exposure time, and seed particles on secondary organic aerosol chemical composition and yield, Atmos.
688 Chem. Phys., 15(6), 3063–3075, doi:10.5194/acp-15-3063-2015, 2015.

689 Lee, A., Goldstein, A. H., Keywood, M. D., Gao, S., Varutbangkul, V., Bahreini, R., Ng, N. L., Flagan, R. C.
690 and Seinfeld, J. H.: Gas-phase products and secondary aerosol yields from the ozonolysis of ten different
691 terpenes, J. Geophys. Res. Atmos., 111(7), 1–18, doi:10.1029/2005JD006437, 2006a.

692 Lee, A., Goldstein, A. H., Kroll, J. H., Ng, N. L., Varutbangkul, V., Flagan, R. C. and Seinfeld, J. H.: Gas-
693 phase products and secondary aerosol yields from the photooxidation of 16 different terpenes, J. Geophys.
694 Res. Atmos., 111(17), 1–25, doi:10.1029/2006JD007050, 2006b.

695 Liu, J., D'Ambro, E. L., Lee, B. H., Lopez-Hilfiker, F. D., Zaveri, R. A., Rivera-Rios, J. C., Keutsch, F. N.,
696 Iyer, S., Kurten, T., Zhang, Z., Gold, A., Surratt, J. D., Shilling, J. E. and Thornton, J. A.: Efficient Isoprene
697 Secondary Organic Aerosol Formation from a Non-IEPOX Pathway, Environ. Sci. Technol., 50(18), 9872–
698 9880, doi: 10.1021/acs.est.6b01872, 2016.

699 Miller, K. A., Siscovick, D. S., Sheppard, L., Shepherd, K., Sullivan, J. H., Anderson, G., L. and Kaufman J.
700 D.: Long-Term Exposure to Air Pollution and Incidence of Cardiovascular Events in Women, N. Engl. J.
701 Med., 356(5), 447–458, doi:10.1002/anie.201206370, 2007.

702 Nannoolal, Y., Rarey, J. and Ramjugernath, D.: Estimation of pure component properties part 3. Estimation of
703 the vapor pressure of non-electrolyte organic compounds via group contribution and group interactions, Fluid
704 Phase Equilib., 269(1–2), 117–133, doi: 10.1016/j.fluid.2008.04.020, 2008.

705 Nah, T., Sanchez, J., Boyd, C. M. and Ng, N. L.: Photochemical Aging of α-pinene and β-pinene Secondary
706 Organic Aerosol formed from Nitrate Radical Oxidation, Environ. Sci. Technol., 50(1), 222–231,
707 doi:10.1021/acs.est.5b04594, 2016.

708 Ng, N. L. and Chhabra, P. S.: Effect ofNOx level on secondary organic aerosol (SOA) formation from the
709 photooxidation of terpenes, Atmos. Chem. Phys., (7), 5159–5174, doi: 10.1016/j.cub.2015.10.018, 2007.

710 Öström, E., Putian, Z., Schurgers, G., Mishurov, M., Kivekäs, N., Lihavainen, H., Ehn, M., Rissanen, M. P.,
711 Kurtén, T., Boy, M., Swietlicki, E. and Roldin, P.: Modeling the role of highly oxidized multifunctional or-
712 ganic molecules for the growth of new particles over the boreal forest region, Atmos. Chem. Phys., 17(14),
713 8887–8901, doi:10.5194/acp-17-8887-2017, 2017.

714 Pankow, J. F. and Asher, W. E.: SIMPOL.1: a simple group contribution method for predicting vapor
715 pressures and enthalpies of vaporization of multifunctional organic compounds, Rev. Mex. Ciencias Farm.,
716 (8), 2773–2796, doi:doi: 10.5194/acp-8-2773-2008, 2008.

717 Pathak, R., Donahue, N. M. and Pandis, S. N.: Ozonolysis of β-pinene: Temperature dependence of secondary
718 organic aerosol mass fraction, Environ. Sci. Technol., 42(14), 5081–5086, doi:10.1021/es070721z, 2008.

719 Pathak, R. K., Stanier, C. O., Donahue, N. M. and Pandis, S. N.: Ozonolysis of α-pinene at atmospherically
720 relevant concentrations: Temperature dependence of aerosol mass fractions (yields), J. Geophys. Res. Atmos.,
721 112(3), 1–8, doi:10.1029/2006JD007436, 2007.

722 Presto, A. A., Huff Hartz, K. E. and Donahue, N. M.: Secondary organic aerosol production from terpene
723 ozonolysis. 2. Effect of NOx concentration, Environ. Sci. Technol., 39(18), 7046–7054,
724 doi:10.1021/es050400s, 2005.

725 Qi, X., Ding, A., Roldin, P., Xu, Z., Zhou, P., Sarnela, N., Nie, W., Huang, X., Rusanen, A., Ehn, M., Rissa-
726 nen, M. P., Petäjä, T., Kulmala, M. and Boy, M.: Modelling studies of HOMs and their contributions to new
727 particle formation and growth: Comparison of boreal forest in Finland and a polluted environment in China,
728 Atmos. Chem. Phys., 18(16), 11779–11791, doi:10.5194/acp-18-11779-2018, 2018.

729 Quéléver, L. L. J., Kristensen, K., Jensen, L., Rosati, B., Teiwes, R., Daellenbach, K. R., Peräkylä, O., Roldin,
730 P., Pedersen, H. B., Glasius, M., Bilde, M. and Ehn, M.: Effect of temperature on the formation of Highly-
731 oxygenated Organic Molecules (HOM) from alpha-pinene ozonolysis, Atmos. Chem. Phys., 1–29,
732 doi:10.5194/acp-2018-1276, 2019.

733 Roldin, P., Ehn, M., Kurtén, T., Olenius, T., Rissanen, M. P., Sarnela, N., Elm, J., Rantala, P., Hao, L., Hytti-
734 nen, N., Heikkinen, L., Worsnop, D. R., Pichelstorfer, L., Xavier, C., Clusius, P., Öström, E., Petäjä, T., Kul-
735 mala, M., Vehkamäki, H., Virtanen, A., Riipinen, I. and Boy, M.: The role of highly oxygenated organic mol-
736 ecules in the Boreal aerosol-cloud-climate system, Nat. Commun., 10(1), 4370, doi:10.1038/s41467-019-
737 12338-8, 2019.

738 Rosenfeld, D., Andreae, M. O., Asmi, A., Chin M., De Leeuw, G., Donovan, D. P., Kahn, R, Kinne, S.,
739 Kivekäs, N., Kulmala, M.,, Lau W., Schmidt K, S., Suni T., Wagner T., Wild, M., and Quaas J., Global obser-
740 vations of aerosol-cloud-precipitation-climate interactions,Rev. Geophys.,52,750–808,
741 doi:10.1002/2013RG000441.

742 Rissanen, M. P., Kurtén, T., Sipilä, M., Thornton, J. A., Kausiala, O., Garmash, O., Kjaergaard, H. G., Petäjä,
743 T., Worsnop, D. R., Ehn, M. and Kulmala, M.: Effects of chemical complexity on the autoxidation
744 mechanisms of endocyclic alkene ozonolysis products: From methylcyclohexenes toward understanding α-
745 pinene, J. Phys. Chem. A, 119(19), 4633–4650, doi:10.1021/jp510966g, 2015.

746 Saathoff, H. and Naumann, K.-H.: Temperature dependence of yields of secondary organic aerosols from the
747 ozonolysis of α-pinene and limonene, Atmos. Chem. Phys., (March), 4–15, doi:10.5194/acp-9-1551-2009,
748 2009.

749 Sarrafzadeh, M., Wildt, J., Pullinen, I., Springer, M., Kleist, E., Tillmann, R., Schmitt, S. H., Wu, C., Mentel,
750 T. F., Zhao, D., Hastie, D. R. and Kiendler-Scharr, A.: Impact of NOxand OH on secondary organic aerosol
751 formation from β-pinene photooxidation, Atmos. Chem. Phys., 16(17), 11237–11248, doi:10.5194/acp-16-
752 11237-2016, 2016.

753 Saunders, S. M., Jenkin, M. E., Derwent, R. G. and Pilling, M. J.: Protocol for the development of the Master
754 Chemical Mechanism, MCM v3 (Part A): Tropospheric degradation of non-aromatic volatile organic
755 compounds, Atmos. Chem. Phys., 3(1), 161–180, doi:10.5194/acp-3-161-2003, 2003.

756 Schmale, J., Henning, S., Henzing, B., Keskinen, H., Sellegri, K., Ovadnevaite, J., Bougiatioti, A., Kalivitis,
757 N., Stavroulas, I., Jefferson, A., Park, M., Schlag, P., Kristensson, A., Iwamoto, Y., Pringle, K., Reddington,
758 C., Aalto, P., Äijälä, M., Baltensperger, U., Bialek, J., Birmili, W., Bukowiecki, N., Ehn, M., Fjæraa, A. M.,
759 Fiebig, M., Frank, G., Fröhlich, R., Frumau, A., Furuya, M., Hammer, E., Heikkinen, L., Herrmann, E.,

760 Holzinger, R., Hyono, H., Kanakidou, M., Kiendler-Scharr, A., Kinouchi, K., Kos, G., Kulmala, M.,
761 Mihalopoulos, N., Motos, G., Nenes, A., O'Dowd, C., Paramonov, M., Petäjä, T., Picard, D., Poulain, L.,
762 Prévôt, A. S. H., Slowik, J., Sonntag, A., Swietlicki, E., Svenningsson, B., Tsurumaru, H., Wiedensohler, A.,
763 Wittbom, C., Ogren, J. A., Matsuki, A., Yum, S. S., Myhre, C. L., Carslaw, K., Stratmann, F. and Gysel, M.:
764 Corrigendum: Collocated observations of cloud condensation nuclei, particle size distributions, and chemical
765 composition, Sci. data, 5, 180094, doi:10.1038/sdata.2018.94, 2018.

766 Shilling, J. E.: Particle mass yield in secondary organic aerosol formed by the dark ozonolysis of α-pinene,
767 Atmos. Chem. Phys., 8(1992), 2073–2088, 2008.

768 Stirnweis, L., Marcolli, C., Dommen, J., Barmet, P., Frege, C., Platt, S. M., Bruns, E. A., Krapf, M., Slowik,
769 J. G., Wolf, R., Prévôt, A. S. H., Baltensperger, U. and El-Haddad, I.: Assessing the influence of NOx con-
770 centrations and relative humidity on secondary organic aerosol yields from α-pinene photo-oxidation through
771 smog chamber experiments and modelling calculations, Atmos. Chem. Phys., 17(8), 5035–5061, doi:10.5194/
772 acp-17-5035-2017, 2017.

773 Tasoglou, A. and Pandis, S. N.: Formation and chemical aging of secondary organic aerosol during the β-
774 caryophyllene oxidation, Atmos. Chem. Phys., 15(11), 6035–6046, doi:10.519

775 Topping, D., Barley, M., Bane, M. K., Higham, N., Aumont, B., Dingle, N. and McFiggans, G.: UMan-
776 SysProp v1.0: an online and open-source facility for molecular property prediction and atmospheric aerosol
777 calculations, Geosci. Model Dev., 9(2), 899–914, doi:10.5194/gmd-9-899-2016, 2016.

778 Waring, M. S.: Secondary organic aerosol formation by limonene ozonolysis: Parameterizing multi-
779 generational chemistry in ozone- and residence time-limited indoor environments, Atmos. Environ., 144, 79–
780 86, doi:https://doi.org/10.1016/j.atmosenv.2016.08.051, 2016.

781 Zhao, D., Schmitt, S. H., Wang, M., Acir, I. H., Tillmann, R., Tan, Z., Novelli, A., Fuchs, H., Pullinen, I.,
782 Wegener, R., Rohrer, F., Wildt, J., Kiendler-Scharr, A., Wahner, A. and Mentel, T. F.: Effects of NOx and
783 SO2 on the secondary organic aerosol formation from photooxidation of α-pinene and limonene, Atmos.
784 Chem. Phys., 18(3), 1611–1628, doi:10.5194/acp-18-1611-2018, 2018.

785 Zhao, D. F., Kaminski, M., Schlag, P., Fuchs, H., Acir, I. H., Bohn, B., Häseler, R., Kiendler-Scharr, A.,
786 Rohrer, F., Tillmann, R., Wang, M. J., Wegener, R., Wildt, J., Wahner, A. and Mentel, T. F.: Secondary
787 organic aerosol formation from hydroxyl radical oxidation and ozonolysis of monoterpenes, Atmos. Chem.
788 Phys., 15(2), 991–1012, doi:10.5194/acp-15-991-2015, 2015.